

Copyright
by
Michael Jaramillo
2020

REVISITING NEUTRON STAR PHYSICS INCLUDING FINITE TEMPERATURE
AND DENSITY EFFECTS ON THE MEDIUM

by

Michael Jaramillo, B.S.

THESIS

Presented to the Faculty of
The University of Houston-Clear Lake

In Partial Fulfillment

Of the Requirements

For the Degree

MASTER OF SCIENCE

in Physics

THE UNIVERSITY OF HOUSTON-CLEAR LAKE

AUGUST, 2020

REVISITING NEUTRON STAR PHYSICS INCLUDING FINITE TEMPERATURE
AND DENSITY EFFECTS ON THE MEDIUM

by

Michael Jaramillo

APPROVED BY

Samina Masood, Ph.D., Chair

Eric Van Mayes, Ph.D., Committee Member

Brandon Reddell, Ph.D., Committee Member

RECEIVED/APPROVED BY THE COLLEGE OF SCIENCE AND ENGINEERING:

David Garrison, Ph.D., Interim Associate Dean

Miguel Gonzalez, Ph.D., Dean

Dedication

This thesis is dedicated to my family, my girlfriend, my friends, and my pets, whose support made all this possible, I love you all to the stars and back. In loving memory of Joseph Otto, whose friendship helped me through my darkest times.

Acknowledgements

I would like to thank the University of Houston Clear Lake and the College of Science and Engineering for providing me with this opportunity to learn and grow. To my committee members Dr. Reddell and Dr. Mayes, thank you for help, advice, and support. To my thesis advisor, Dr. Masood, I could not have completed this without your unwavering support and understanding. You understood and respected my independence while also making sure I felt fully integrated into the research group. Your reassurance and kind words made me feel like completing this was always within my grasp.

ABSTRACT

REVISITING NEUTRON STAR PHYSICS INCLUDING FINITE TEMPERATURE AND DENSITY EFFECTS ON THE MEDIUM

Michael Jaramillo
University of Houston-Clear Lake, 2020

Thesis Chair: Samina Masood, Ph.D.

Neutron stars are highly compact stellar evolutionary endpoints whose formation and existence rely on a complex interplay between the overall hydrodynamic equilibrium and the local approach of quantum mechanics. The extreme conditions theorized inside neutron stars seems to set up conditions for the existence of exotic forms of matter. This project aims to develop a better understanding of the dynamics of neutron stars with the eventual goal of developing an improved and testable model for neutron stars. We begin with a brief review of stellar evolution, from molecular cloud, all the way up to core collapse supernovae, where the temperature and densities begin to take on extreme values. We look at weak force interactions during the supernova and then examine their role in determining the equation of state and thermal evolution of a neutron star. We discuss the structure of neutron stars and the different varieties of neutron star systems that have been observed. Finally, we examine the modification of electron properties in the finite temperature and densities encountered in the interiors of neutron stars. We look

at the number density of electrons in high temperatures and chemical potentials in the context of neutron star thermal evolution and find that it fits with existing cooling trends.

TABLE OF CONTENTS

List of Tables	x
List of Figures	xi
CHAPTER I: INTRODUCTION.....	1
1.1 Introduction.....	1
1.2 Historical Background	2
CHAPTER II: STELLAR FORMATION AND EVOLUTION	7
2.1 Stellar Formation: From Gas Cloud to Protostar	7
Jeans Criterion	7
Types of Collapse	9
Role of Magnetic Fields in Collapse.....	9
Cloud Fragmentation	10
2.2 Protostar Evolution and Pre-Main-Sequence.....	10
2.3 Stellar Evolution and HR Diagram	12
2.4 Evolution of Low and Medium Mass Stars	13
Low Mass.....	13
Medium Mass.....	16
2.5 Evolution of High Mass Stars	16
CHAPTER III: SUPERNOVA AND NEUTRINO PROCESSES	18
3.1 Supernova	18
3.2 Types of Supernova	20
3.3 Neutrino Production during collapse	21
3.4 Neutrino Opacity.....	23
3.5 White Dwarfs and Chandrasekhar Limit	25
CHAPTER IV: NEUTRON STARS	32
4.1 Introduction to Neutron Stars.....	32
4.2 Neutron Star Structure	32
4.3 Regions	32
Surface and Envelope	33
Outer Crust.....	33
Inner Crust	34
Core.....	35
4.4 Types of Neutron Stars	35
Pulsars.....	35
Magnetars.....	40

Quark Stars.....	40
CHAPTER V: EQUATIONS OF STATE AND BETA PROCESSES.....	42
5.1 Introduction to Neutron Star Equations of State.....	42
5.2 Observational Constraints.....	43
Mass Measurements.....	44
Radius Measurements.....	47
Mass-Radius Relationship.....	48
5.3 Equation of State Below Neutron Drip.....	49
Ideal Cold Neutron Gas.....	49
5.4 Inverse Beta Decay Correction to EOS.....	53
5.5 Thermal Evolution of Neutron Stars.....	57
URCA Process and Protoneutron Stars.....	58
Modified URCA Process.....	59
CHAPTER VI: EXAMINING BETA PROCESSES THROUGH QED IN HOT AND DENSE MEDIUM.....	60
6.1 Introduction to equations.....	62
6.2 Evaluating and Discussing the Number Density.....	64
Discussions and Conclusions.....	71
6.3 Future Work.....	73
REFERENCES.....	74

LIST OF TABLES

Table 1: Pre-main sequence contraction times for classical models. Source: [9] (table 12.1 from C&O p427).....	12
Table 2: Temperatures in Kelvin and MeV for stages of neutron star evolution	65

LIST OF FIGURES

<p>Figure 1: Evolutionary tracks for protostars of different masses that have a composition $X=0.68$, $Y=0.30$, $Z=0.02$. The Hayashi track is the almost vertical part on the right side of a track. Track for a given mass goes from right to left. Source: [9].....</p>	11
<p>Figure 2: Evolutionary tracks for stars of various masses from their ZAMS. Source: [9].....</p>	13
<p>Figure 3: Evolutionary path of one solar mass star from ZAMS. Source [9] (figure 13.4 C&O).....</p>	14
<p>Figure 4: Evolutionary path of 5 solar mass star from ZAMS. Source: [9].....</p>	16
<p>Figure 5: Cross sectional diagram of two $1.4 M_{\odot}$ neutron stars. Reid EOS on left, TNI EOS on the right. Source [40]</p>	33
<p>Figure 6: Misalignment of magnetic axis and rotation axis in a pulsar, includes field lines and emission of radio beam. Source: https://www.cv.nrao.edu/course/astr534/images/PSRs_pulsar_sketch.png</p>	36
<p>Figure 7: Plot of many pulsar spin periods vs magnetic field strength. Source: https://astronomy.swin.edu.au/cms/cpg15x/albums/userpics/pulsarevolution2.jpg</p>	37
<p>Figure 8: Pulsar Map of the Sun's relative position engraved on Pioneer and Voyager probes. Source: https://to-the-stars-web-assets.s3.amazonaws.com/files/Pulsar%20Map.jpg</p>	39
<p>Figure 9: Generation of $M(R)$ curve from a specific EOS $p(\epsilon)$. $\epsilon_s \approx 150 \text{ MeV fm}^{-3}$ is the energy density at the nuclear saturation density $n_s \approx 0.16 \text{ fm}^{-3}$. Source [18].</p>	43
<p>Figure 10: Mass distribution for different populations of neutron stars. Source [28].....</p>	45
<p>Figure 11: Measured neutron star masses sorted by type of system. Source [28]</p>	46
<p>Figure 12: Mass-central density relation and mass-radius relation for various neutron star EOS. Source: [40]</p>	49
<p>Figure 13: Electron number densities for defined chemical potential range and temperatures from Table 1.....</p>	66
<p>Figure 14: Electron number densities for defined chemical potential range and temperatures from Table 1 with logarithmic scale on chemical potential</p>	67
<p>Figure 15: Graph of n_e vs μ at constant temperatures for an expanded range of temperatures</p>	68
<p>Figure 16: Graph of n_e vs μ for constant temperatures with log scale on chemical potential for expanded temperatures</p>	69

Figure 17: Graph of n_e vs μ for constant temperatures with negative n_e values included.....	70
Figure 18: Graph of n_e vs μ for constant temperatures with log scale on chemical potential and negative n_e values included.....	71

CHAPTER I:
INTRODUCTION

1.1 Introduction

Neutron stars are extremely dense stellar remnants with masses between 1-3 solar masses and radii of around 12km [17]. They are highly degenerate objects that may represent one of the final stages of stellar evolution for high mass stars that do not have enough mass to become black holes. Neutron stars represent a unique type of objects with unusual microscopic properties that govern the overall behavior of the star. This interplay between vastly different scales gives unique properties to neutron stars and make them both fascinating and complex systems.

Neutron stars are excellent laboratories to study extreme conditions that are not currently replicable on Earth. Their gravitational effects on spacetime and binary partners also offer unprecedented tests of Einstein's general theory of relativity [11]. The conditions in the interior of neutron stars may allow for exotic states of matter such as metamaterials, high temperature superfluids, or quark matter in a quark-gluon plasma phase. Equations of state which describe the composition and interactions in neutron stars can be examined to find the minimum and maximum radii and mass of neutron stars supported by that model. By comparing the properties of observed neutron stars with the predicted ranges from equations of state, the internal properties and composition of neutron stars can be inferred.

Beta processes, electron capture by proton and neutron decay, are responsible for the conversion of protons and electrons into neutrons and the emitted neutrinos are the dominant cooling mechanism. When it comes to understanding neutron stars and their structural evolution, understanding the beta processes is of the utmost importance. The

high energy electrons, already occupying all the available energy levels, can block neutron decay when the neutron star is cooled down to a lower temperature. However, the local behavior of the high energy nuclear matter of neutron is dealt with as a relativistic quantum system. We apply QED (quantum electrodynamics) and Fermi-Dirac statistics to the electron gas in a hot and dense background to determine the evolution of electron occupancy with changing chemical potential and temperature. This gives a deeper insight into the thermal evolution of the neutron star and the composition of the interior of the star.

1.2 Historical Background

The theoretical work on neutron stars began even before the neutron was discovered. Landau was one of the first to predict the existence of a more compact state of stellar matter when in sufficient densities [46]. Landau's assertion in 1932 was groundbreaking, as the neutron was not yet discovered and helped spur interest in the field.

A couple years later, in 1934, astronomers Baade and Zwicky proposed that supernovae may represent "the transition of an ordinary star into a body of considerably smaller mass" [8]. They also correctly predicted that the supernova are powered by the release of gravitational binding energy [8].

The next major advancement in the study of neutron stars came 5 years later in 1939 from Tolman, Oppenheimer, and Volkoff [27]. They suggested that because of the density of the stellar matter, it may be possible to form a new phase of matter consisting primarily of neutrons. They assumed that the neutrons behaved as an ideal gas when at high density and solved the equation of states for an ideal, relativistic, cold Fermi gas [27]. Their equations had incorporated the general relativistic approach due to the density of the compact object and the curved space-time around the object. These equations are

known as the Tolman-Oppenheimer-Volkoff (TOV) equations and represent the first attempts to define the structure of relativistic stars. They are the basis of current attempts to model the structure and interior physics of neutron stars. Using the TOV equations, one can predict the total mass, density, and radius of a star. They found a mass range for neutron stars of $\frac{1}{3}$ solar masses $< m < 0.7$ solar masses, below the Chandrasekhar limit. This is due to limited understanding of nuclear matter and the strong nuclear force at the time. When the strong nuclear repulsion forces are accounted for, the mass range becomes 1.5 solar masses $< m < 3$ solar masses, a much more realistic estimate [40].

Unfortunately, much of the other work on degenerate neutron dominated objects at the time was focused on the possibility that neutron cores could provide a source of energy for high mass stars [40]. It was thought that because of the small surface area, any thermal radiation from a neutron star would be too faint to be detected optically [34],[40]. These two notions caused further work on neutron stars to stall for several years.

Later on, the interest in the study of neutron star and their potential properties was renewed with the discovery of the first nonsolar X-ray source [12]. It was initially speculated that this signal could originate from a young and still warm neutron star. This led to several approaches to calculate the cooling rates of neutron stars based on the properties of the observed X-ray source. Then in 1963, the first quasi-stellar object was discovered by Schmidt using the observatory at Mount Palomar [36]. This object, which later turned out to be a galaxy at very high z , was of particular interest because its spectral lines were greatly redshifted. The cause of the redshift was unknown and was at first considered to be from the enormous gravitational energy at the surface of a compact object like a neutron star. Eventually though, it was determined that the amount of redshift exceeded the maximum gravitational potential at the surface of a neutron star [38].

In 1964, Lodewijk Woltjer reasoned that the magnetic fields would be amplified during the collapse and formation of neutron stars due to magnetic flux conservation [45]. He estimated that field strength could be as high as 10^{16} G [45]. Then in 1967, astrophysicist Franco Pacini proposed that if neutron stars were rotating and had large magnetic fields, then they would emit electromagnetic radiation from particles accelerated by the magnetic fields [29]. These particles would also serve to power their surrounding nebula.

Also in 1967, Jocelyn Bell, a graduate student under the supervision of Anthony Hewish, detected a weak, repeating radio source [15]. The signal had periodic pulses of 1.337 seconds and was originally nicknamed LGM, Little Green Men, as it was thought it could have been a signal from an alien civilization. Shortly after however, a second source was found in a completely different part of the sky, and thus, the alien civilization proposal was abandoned. The object was eventually identified as a new type of star, thought to be somewhere between a white dwarf and neutron star and rotating rapidly. The name pulsar arose from a portmanteau of pulsating and quasar. It was Gold who proposed in 1968 that pulsars are rapidly rotating neutron stars [13]. 1968 also saw the back-to-back discoveries of a pulsar in the Crab Nebula and of a pulsar in the constellation Vela. The Crab Nebula pulsar was of particular interest because Chinese astronomers observed the supernova, responsible for the remnant, in the year 1054 AD [40]. This meant that the age of this particular neutron star was more accurately known than most others and offered a unique chance to look at the evolution of a relatively young neutron star.

The late 1960's and early 1970's saw a flurry of theoretical and observation work dedicated to understanding the properties of neutron stars. The Uhuru satellite discovered the first pulsating and compact sources of X-rays. Because of previous theoretical work,

it was thought that these pulsating X-ray sources were from neutron stars in close binary systems that were in the process of accreting material from their companion star and onto their surface. This theoretical work was confirmed by observations of the sources Cen X-3 and Her X-1 [37].

Improvements in optics and data analysis has significantly helped advance the study of neutron stars in the last few decades. The Chandra X-ray Observatory, launched in 1999, was far more sensitive to X-ray emissions than previous X-ray telescopes. Chandra's first light observation was of an X-ray point source in the center of the Cassiopeia A supernova remnant. It is believed that the supernova that formed the Cassiopeia A remnant was first observed in 1680 [5]. Researchers compared the observed spectrum to several spectral models and concluded the source was likely a strongly magnetized neutron star with two hot spots with $T = 2.8 \text{ MK}$ or $T = 0.241 \text{ MeV}$ on a cooler surface of $T = 1.7 \text{ MK}$ or $T = 0.146 \text{ MeV}$ [32]. These temperatures are in agreement with existing neutron star cooling models based on the estimated date of the supernova.

The Neil Gehrels Swift Observatory was launched in 2004 with the mission of observing gamma-ray bursts and their afterglow in X-ray and UV. Among other sources, gamma-ray bursts are thought to also be associated with several types of neutron star systems and events. Swift has been used to observe high mass X-ray binary systems, where a massive star overflows its Roche lobe during its stellar evolution and is accreting matter onto the surface of a neutron star. The accreted matter is accelerated along magnetic field lines and then collides with the surface, converting potential energy into heat. The regions where accreted matter strikes the surface produces X-ray hotspots, which rotate with the neutron star's rotational period, giving the appearance of periodic X-ray pulsation [16].

However, one of the most powerful tools for probing the properties of neutron stars and other massive, compact objects does not rely on electromagnetic radiation. Instead, researchers at the Laser Interferometer Gravitational-Wave Observatory (LIGO) and Virgo have found a way to measure the spatial disturbance of passing gravitational waves produced by the merging of compact objects like neutron stars and black holes. When a signal is detected and found to be a possible candidate for a compact object merger, LIGO sends out an alert to research telescopes to look for an electromagnetic counterpart to the merger [10]. The first optical counterpart from a gravitational wave detection of a neutron star merger was confirmed in 2017 and provided scientists with a plethora of valuable data. The merger was found to have produced many of the heavy elements such as gold that are not produced through fusion during a star's lifespan.

CHAPTER II:
STELLAR FORMATION AND EVOLUTION

2.1 Stellar Formation: From Gas Cloud to Protostar

Stellar dynamics can be described in terms of a constant battle of two opposing forces: inwards gravitational attraction and outwards radiative pressures. The life and death of a star is associated with the production and distribution of the elements thought to be required for life. Thus, understanding the process of stellar formation and evolution is crucial for understanding how both compact objects form and how heavy elements are distributed in the universe.

Stars are formed inside a large-dense cloud of gas and dust, called nebula. In the low temperatures of the interstellar medium, 10-100K, hydrogen atoms can form a molecular bond to create molecular hydrogen as H_2 . The virial theorem,

$$2K + U = 0, \tag{2.1}$$

describes the necessary conditions to initiate the formation of a star. If the internal energy (thermal, kinetic, etc.), $2K$, of the cloud is greater than the gravitational potential of the cloud, U , then the cloud will expand. However, if the gravitational potential is greater than the internal energy, the cloud will begin to collapse.

Jeans Criterion

Sir James Jeans developed some criteria necessary for the cloud to begin collapsing into a protostar in 1902 [9]. We begin by considering a spherical cloud of uniform density, composed solely of molecular hydrogen, so the gravitational potential energy can be written as

$$U \sim - \frac{3}{5} \frac{GM_c^2}{R_c} \tag{2.2}$$

where the subscript ‘c’ denotes properties of the cloud, such as mass and radius. The internal energy is given by

$$K = \frac{3}{2}NkT, \quad (2.3)$$

where N is the total number of particles in the system. N is given by

$$N = \frac{M_c}{\mu m_H}, \quad (2.4)$$

where μ is the mean molecular weight and m_H is the mass of hydrogen. The virial theorem and conditions for collapse can then be combined to describe the condition for the formation of a star as

$$\frac{3M_c kT}{\mu m_H} < \frac{3}{5} \frac{GM_c^2}{R_c}. \quad (2.5)$$

By replacing R_c with an expression in terms in the initial density of the cloud (assumed to be constant throughout the cloud), such that

$$R_c = \left(\frac{3M_c}{4\pi\rho_0} \right)^{1/3}, \quad (2.6)$$

then Eq. (2.5) can be solved for the minimum mass needed to begin the gravitational collapse of the cloud. This mass is called the Jean’s Mass and makes up half of the Jeans criterion. The Jeans Mass can be expressed as

$$M_J \simeq \left(\frac{5kT}{G\mu m_H} \right)^{3/2} \left(\frac{3}{4\pi\rho_0} \right)^{1/2}. \quad (2.7)$$

The other half of the Jeans criterion is the Jeans Length, and it describes the radius at which the cloud needs to be at in order for gravitational collapse to proceed. It is given by the expression

$$R_J \simeq \left(\frac{15kT}{4\pi G\mu m_H \rho_0} \right)^{1/2} \quad (2.8)$$

M_J and R_J represent the mass radius, respectively, and provide the conditions for the gravitational collapse in Eqs. (2.7 and 2.8).

Types of Collapse

There are several ways for the collapse of the cloud to proceed. The simplest case is that of homologous collapse. In homologous collapse, factors in the collapse such as rotation of the cloud, the presence of turbulence within, or the magnetic field interactions are ignored. It is also assumed that any existing pressure gradient is too small to noticeably impact the motion of the cloud during collapse [9]. It can then be said that all parts of the cloud are in freefall and take the same amount of time to collapse. Therefore, the density is increasing at the same rate for all parts of the collapsing cloud, hence the name homologous collapse.

If the cloud begins with an uneven density distribution, like a denser central region, then the free-fall time will vary with distance from the center of collapse. This type of collapse is known as inside-out collapse.

Role of Magnetic Fields in Collapse

The above derivations ignored the energy contributions of magnetic fields in the collapsing cloud, but we know the magnetic field is there. Measurements of molecular clouds found fields with strengths around 1 to 100 nT [9]. The presence of a magnetic field in the cloud means that as the collapse of the cloud proceeds, the magnetic field strength will increase, and the increasing field strength will cause resistance to the compression of the cloud through repulsive magnetic interactions. Incorporating the magnetic field into the virial theorem yields a critical mass of the cloud

$$M_B = c_B \frac{\pi R^2 B}{G^{1/2}} \quad (2.9)$$

where c_B is given by

$$c_B = 380 N^{1/2} m^{-1} T^{-1}. \quad (2.10)$$

If the mass of the cloud is below M_B , it will be stable against collapse, and the cloud is said to be magnetically subcritical. If the mass exceeds M_B , then the force of gravity will overcome the magnetic field resistance to collapse and it is said to be magnetically supercritical.

Cloud Fragmentation

Molecular clouds can have masses well in excess of hundreds of solar masses, so why do these clouds not collapse into one or several supermassive stars? The answer lies in the distribution of mass in the cloud. We earlier assumed a uniform distribution of mass in the molecular clouds, for simplicity. However, in reality, these clouds have inhomogeneities in density which will cause individual parts of the cloud to satisfy the Jeans criterion and begin their collapse locally. These individual collapsing sections cause the cloud to break apart and fragment into many smaller pieces.

2.2 Protostar Evolution and Pre-Main-Sequence

As the collapse of the cloud proceeds and the density rises, the central temperature begins to increase. When the internal temperature reaches about 2000K [9], the molecular hydrogen begins to break apart into individual atoms. This process absorbs energy and removes the pressure gradient that was maintaining hydrostatic equilibrium in the cloud, causing the cloud to continue collapsing inwards. The core of the protostar will collapse to a radius of about 30% of the Sun's present size, where it will achieve temporary hydrostatic equilibrium again. The core begins to accrete additional matter and eventually reaches an internal temperature where deuterium can start burning. This reaction proceeds before hydrogen burning as it has a larger cross section at lower temperatures. The luminosity of the protostar is fairly constant during this phase of evolution.

The deuterium in the core depletes quickly and the luminosity of the protostar drops and the protostar settles into the Hayashi track. The Hayashi Track is an evolutionary path that collapsing protostars follow as they maintain hydrostatic equilibrium.

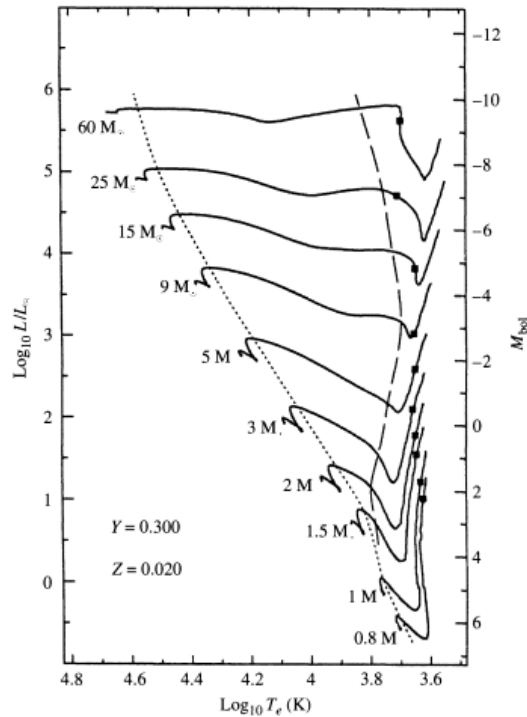


Figure 1:
Evolutionary tracks for protostars of different masses that have a composition $X=0.68$, $Y=0.30$, $Z=0.02$. The Hayashi track is the almost vertical part on the right side of a track. Track for a given mass goes from right to left. Source: [9]

As the temperature of the protostar rises, the outer layers become dominated by the presence of H^- ions and free electrons, coming from partially ionized heavier elements. This significantly raises the opacity and causes the outer layers to become convective. The overall effect of the outer layer opacity is to slow the rate of collapse. But as the effective temperature rises, the core becomes radiative and grows in mass. The core of the protostar undergoes several adjustments, temporarily reaching temperatures high enough to allow the first two steps in hydrogen burning and for carbon to burn into

nitrogen, but not at equilibrium rates. Eventually, the luminosity decreases, the effective temperature decreases, and the core is composed primarily of hydrogen. This marks the end of the protostar evolution and the beginning of the star's time on the main sequence of the HR Diagram. The moment when a star joins the main sequence is known as the Zero Age Main Sequence (ZAMS).

Protostars with larger masses evolve quicker than lower mass protostars while also undergoing different evolutionary phases on their way to the main sequence.

Initial Mass (M_{\odot})	Contraction Time (Myr)
60	0.0282
25	0.0708
15	0.117
9	0.288
5	1.15
3	7.24
2	23.4
1.5	35.4
1	38.9
0.8	68.4

Table 1:
Pre-main sequence contraction times for classical models. Source: [9] (table 12.1 from C&O p427)

2.3 Stellar Evolution and HR Diagram

The Hertzsprung-Russell Diagram is a scatter plot composed of many stars that compares a star's luminosity to its effective temperature. Luminosity can be divided into spectral types: O, B, A, F, G, K, and M. By plotting a large number of stars with various masses, trends begin to emerge. One of the obvious trends is known as the main sequence, the curve along which stars burning hydrogen into helium in their core can be placed. Stars spend the majority of their lives in the main sequence. As a star evolves, its luminosity and effective temperature change, along with its placement on the HR

diagram. Stars of the same mass and composition will follow the same evolutionary tracks on the HR diagram.

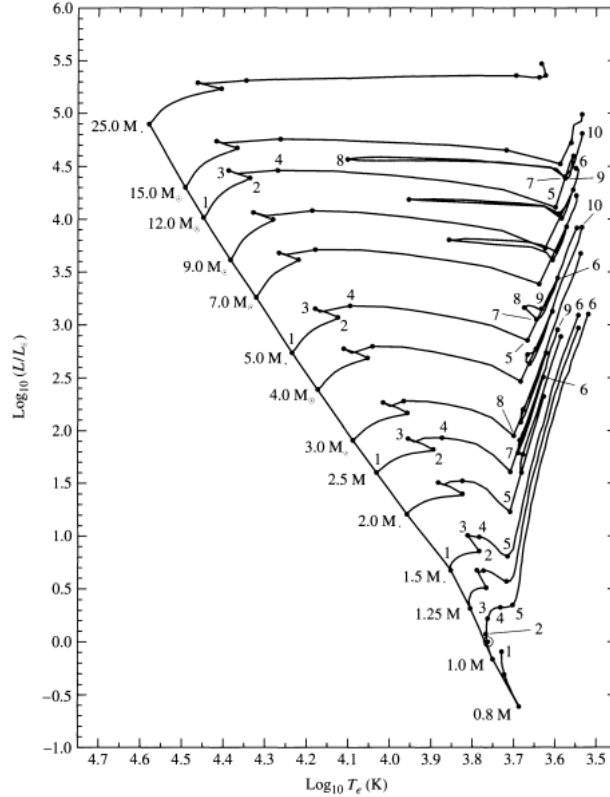


Figure 2:
Evolutionary tracks for stars of various masses from their ZAMS. Source: [9]

2.4 Evolution of Low and Medium Mass Stars

Low Mass

The dominant nuclear reaction in zero age main sequence stars with masses less than $1.2M_{\odot}$ is hydrogen burning through the proton-proton, or ‘pp’, chain. This process continues until all the hydrogen in the core is depleted, leaving an inert helium core. Without the radiative pressure from hydrogen burning, the core contracts. Hydrogen shells around the core can then begin burning, causing the star to expand and increase in luminosity. This expansion causes the effective temperature to lower, thus reddening the

star. However, the expansion is not as great as later stages, so this phase is known as the sub giant branch.

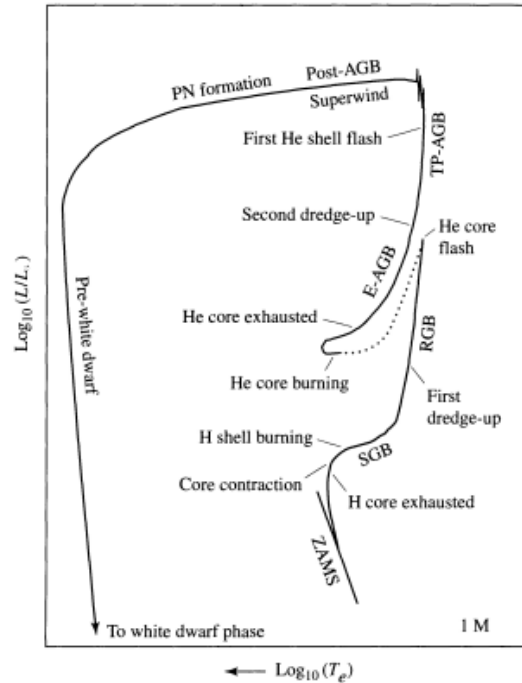


Figure 3:
Evolutionary path of one solar mass star from ZAMS. Source [9] (figure 13.4 C&O)

As hydrogen shell burning progresses, energy is quickly released. With the lowered temperature and the expanded stellar envelope, the opacity of the outer layers increases, causing a convection zone near the surface. This convective zone efficiently transports energy to the surface of the star to be radiated away. This causes the star to continue expanding and moving up what is known as the red giant branch. The convective zone also leads to material from the interior to appear on the surface, altering the spectral emissions from the surface.

As the star evolves along the red giant branch, its helium core continues to contract until the electrons become degenerate. There is also significant energy loss in the

form of neutrinos escaping from the core. When the core becomes dense and hot enough, conditions become favorable for the triple alpha process to take place. The triple alpha process is the process through which two helium-4 nuclei combine into beryllium-8, which then fuses with another helium-4 nuclei into carbon-12. This process relies on the probability of the last step since beryllium-8 is unstable, and so requires a hotter core. The triple alpha process releases a large amount of energy in a short amount of time. The helium ignites first in a shell around the core, but quickly spreads to the whole core. For only a few seconds, the star reaches a luminosity on the order of $10^{11}L_{\odot}$. This is known as the helium core flash. However, the thermally expanding core and the outer layers absorb most of the released energy before reaching the surface, leading to small amount mass loss from the surface. Because the helium flash is so quick, stellar evolutionary calculations for this step require very small timesteps and a detailed understanding of all the processes occurring.

The expansion of the core during the helium flash lowers the rate at which the hydrogen shells are fusing and causes the star to contract. It is at this stage, with decreasing radius and increasing surface temperature, that it is on the horizontal branch. After the helium is depleted in the core, leaving a carbon-oxygen core, there are still hydrogen and helium shells burning, with hydrogen burning producing the majority of the energy. Helium from hydrogen shell burning periodically settles towards the core, where it also ignites in what is known as a thermal pulse.

Once the shells have burned through their fuel and the core is composed of carbon and oxygen, the star is no longer capable of producing enough radiative energy to support itself against gravitational collapse. More massive stars are able to start carbon burning and continue their evolution, but for stars near $1M_{\odot}$, this marks the end of the nuclear burning. The star rapidly loses mass in the form of superwinds, with mass loss rates up to

$10^{-4} M_{\odot}$ per year. This wind produces a planetary nebula around the cooling core, which eventually becomes a white dwarf. The planetary nebula is rich in heavy elements such as carbon, sulfur, and oxygen [9].

Medium Mass

The evolutionary path of a $5M_{\odot}$ star is a little different than a $1M_{\odot}$ star. Not only does the stellar evolution proceed at a quicker rate than in low mass stars, it also undergoes further nuclear burnings. The additional mass causes the core to be denser and hotter, which increases the rate at which nuclear reactions occur in the core. Medium mass stars go through the same initial stages as low mass stars but have more pronounced sub giant branches and horizontal giant branches due to extended shell burning periods.

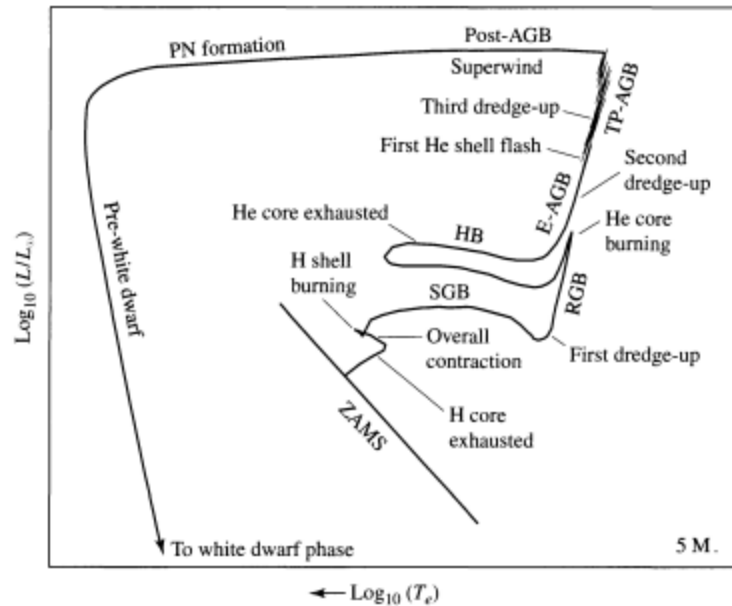


Figure 4:
Evolutionary path of 5 solar mass star from ZAMS. Source: [9]

2.5 Evolution of High Mass Stars

Massive stars ($8 - 10 \leq M/M_{\odot} \leq 70$) also evolve more quickly than low and medium mass stars, with average lifetimes around 10^5 years [24]. Due to their larger

mass, the cores of massive stars are able to undergo further nuclear burning processes than their smaller mass brethren. As with all stars, fusion in the core begins with the *pp*-chain fusing hydrogen into helium. It is during this phase of nuclear burning that the star is said to be on the main sequence of the HR diagram. Once hydrogen fusion in the core ceases, the core will contract and heat up due to the release of gravitational potential energy, thus creating the conditions for helium fusion through the triple alpha process.

The carbon burning stage happens after the oxygen burning stage and begins when the core is composed of mostly silicon and sulfur. The core will contract, and the temperature of the core will rise to 2.7-3.5 GK or 30-300 keV through the release of gravitational energy. These high temperatures cause some of the elements in the core to undergo photodisintegration, leading to an abundance of alpha particles. These alpha particles then fuse with available silicon to form Sulfur-32, all the way up to Nickel-56. The silicon burning stage is very short lived, lasting approximately one day [9]. The star is now dynamically unstable and will undergo a violent, explosive death known as a supernova, leaving behind a type of compact object such as a black hole or neutron star.

CHAPTER III:
SUPERNOVA AND NEUTRINO PROCESSES

3.1 Supernova

A special category of stellar objects are superdense systems such as supernova and neutron stars. These are extremely dense systems with extreme statistical conditions, which follow unique dynamics. Understanding the dynamics of supernova gives insight into the conditions of the protoneutron star. Neutrinos produced during the supernova and by reactions in the protoneutron star can provide detailed information about the mechanisms at play in these superdense systems.

Supernovae are some of the most energetic and powerful events in the universe, sometimes having a peak brightness that temporarily outshines the entire output of their host galaxy [26]. There are two types of supernova, Type I and Type II. With the exception of Type Ia supernovae, they are the cataclysmic, end-of-life explosions of massive stars after the stars have run out of nuclear fuel and cannot support themselves against gravitational collapse.

In order for a star to undergo a supernova explosion, its initial mass needs to be greater than $8-10M_{\odot}$ [17]. Because of the additional mass, the core is able to undergo further nuclear reactions than the cores of lower mass stars. At the end of each fusion cycle, the core is no longer producing enough radiative pressure to counteract the effects of gravity, which then causes the core to contract, reaching higher temperatures and densities. These contractions create the conditions needed for the fusion of heavier elements and the core proceeds like this until it reach high enough temperatures ($T_c \approx 8.0 \times 10^9 K$) and densities ($\rho_c \approx 10^9 g/cm^3$) to fuse silicon into ${}^{56}_{26}\text{Fe}$ [9]. Any further fusions would require more energy to fuse than it releases (endothermic) and now the final collapse of the core begins.

With the rising temperature of the core, photons in the core now have enough energy, which is around 124.4MeV, to break apart the iron nuclei in a process known as photodisintegration.



This process is also endothermic and rapidly reduces the pressure from the thermal energy of the gas, driving the collapse onwards. When the temperature reaches $T_c \approx 11 \times 10^9 K$, the alpha particles also begin to photodisintegrate into free protons and neutrons.



Both photodisintegration processes do not proceed completely, and the presence of heavy nuclei still needs to be accounted for. It cannot be assumed that core is a complete ball of iron, nor can it be assumed the core is completely photodisintegrated.

The star has always been very hot and so the electrons of the atoms have been ionized and free moving since the star began fusing hydrogen. Because electrons are fermions and are subject to the Pauli Exclusion Principle, they are forced to occupy higher and higher energy levels as the temperature rises. The maximum energy level of electrons is known as the Fermi Energy. As the highest energy level approaches the Fermi Energy, the electrons become relativistic. This increasing energy requirement provides hydrodynamic pressure to counterbalance the gravitational pull. The core, which was still partially being supported by electron degeneracy pressure, now has an excess of free protons which are quickly converted into neutrons by the relativistic electrons [40]. The electron degeneracy pressure is now gone, and the protons and electrons of the core are rapidly converted into neutrons. Neutrons are also fermions and have their own corresponding degeneracy pressure.

Depending on the initial mass of the star, and its current core mass during disruption, the core may collapse into a neutron star or further into a black hole. In the case of neutron star formation, the collapse of the core is only halted by the pressure of degenerate neutrons. It is not currently known whether there is an in-between state for stellar remnants, some have hypothesized the existence of quark stars, held up by the pressure of degenerate quarks.

During the collapse of a massive star's core, massive amounts of neutrinos are produced, primarily through two types of processes: neutronization and thermal emission. Neutrinos have a very low cross section of interaction and they can pass through the layers of the star and stream into space, carrying away significant amounts of energy, as well as detailed information about the physics of where they were created. Photons produced in the core will have gone through many random walks, periods of absorption and reemission, and scattering incidents. These interactions will cause the photon to lose the information of its creation, but neutrinos produced in the core are able to stream out of the core with the information of their creation intact [22].

3.2 Types of Supernova

Supernova are classified based upon their spectral emission lines into two main categories: Type I and Type II. The distinction between the two is that Type I lack hydrogen emission lines while those lines are present in Type II. Type I can be further broken up into the Ia, Ib, and Ic subcategories. Type Ia has a strong singly ionized silicon line at 615.0 nm, which is near the peak light, while Type Ib and Ic both lack or have very weak lines at that wavelength. Type Ib and Ic can be differentiated by a non-ionized helium line at 587.6 nm, which Ib has and Ic either lacks this line or it is weak in the spectra. The absence of hydrogen emission lines in Type I supernova imply that the stars involved have had their hydrogen envelopes stripped away [9].

Type Ia supernova have been observed in both elliptical and spiral galaxies, while Type Ib and Ic are typically only found near regions of star formation in spiral galaxies. This indicates that Type Ia supernova are from longer lived or end of life stellar remnants and that Type Ib and Ic are from shorter lived, more massive stars [9]. It is now understood that Type Ia are caused by a binary system where a white dwarf accretes material from its companion star until the white dwarf exceeds the Chandrasekhar limit, which is about $1.44M_{\odot}$.

Type II supernova all initially show hydrogen emission lines, with the majority of subcategories maintaining those hydrogen emission lines through the supernova. The one exception is Type I Ib supernova, which have spectra that change part way through to resemble the spectra of Type Ib.

3.3 Neutrino Production during collapse

During the collapse of a massive star's core, massive amounts of neutrinos are produced, primarily through two types of processes: neutronization and thermal emission. Neutrinos have a very low cross section of interaction and they can pass through the layers of the star and stream into space, carrying away significant amounts of energy, as well as detailed information about the physics of where they were created. Photons produced in the core will have gone through many random walks, periods of absorption and reemission, and scattering incidents. This causes the photon to lose the information of its production, but neutrinos with their low cross section of interaction can be formed then escape without interaction [22].

Thermal emissions take place before the core collapse, so we will discuss those processes first. The primary thermal emission processes are electron-positron pair annihilation, photoannihilation, and Bremsstrahlung. These three reactions can all

proceed through exchanges of either a charged current of W^\pm vector bosons or a neutral current of Z bosons.

Electron-positron pair annihilation occurs with both the real and virtual electron positron pairs and forms a neutrino-antineutrino pair. Pair annihilation of electron-positron pairs typically produce electron neutrino pairs, through an exchange of a W^\pm boson, but can also produce pairs of the heavy varieties of neutrinos, the muon and tau neutrinos, and their corresponding antineutrinos through an exchange of the Z boson.

$$e^+ + e^- \xrightarrow{(W, Z)} \nu + \bar{\nu} \quad (3.3)$$

Photoannihilation occurs when an electron collides with a gamma ray and produces a neutrino-antineutrino pair.

$$e^- + \gamma \xrightarrow{(W, Z)} e^- + \nu + \bar{\nu} \quad (3.4)$$

Thermal Bremsstrahlung, also known as free-free emission, is the process through which a relativistic electron inelastically scatters off a nonrelativistic ion or non-relativistic electron.

$$e^- + (Z, A) \xrightarrow{(W, Z)} (Z, A) + e^- + \nu + \bar{\nu} \quad (3.5)$$

Neutronization is the broad term for the two processes in which protons combine with electrons. Neutronization is most significant when the core collapse has fully begun as each reaction reduces the fraction of free electrons, and thus, the electron degeneracy pressure that was counteracting gravitational collapse. As the density increases and electron fraction decreases, the mass number A , the proton number Z , and the neutron number $N = A - Z$ all increase. The most common is simple electron capture by nuclei, where a proton rich nucleus absorbs an electron [40].

$$e^- + (Z, A) \xrightarrow{(W)} \nu_e + (Z - 1, A) \quad (3.6)$$

The other neutronization process, electron capture by free protons, is less common, but is still present and must be accounted for.



It eventually becomes the dominant neutronization process when the average neutron number per nuclei exceeds 40 [40].

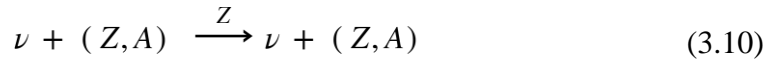
3.4 Neutrino Opacity

Neutrinos are able to freely stream out of the collapsing star at the beginning of the collapse due to their low cross section of interaction and lower density of the star at that time. However, as the collapse proceeds and the density increases, the possibility of neutrino absorption and scattering processes increases and the material becomes partially opaque to neutrinos. The absorption and scattering processes are free nucleon scattering, coherent scattering by heavy nuclei, nucleon absorption, and electron-neutrino scattering. Parallel processes also occur for the antineutrinos in the core [40].

Free nucleon scattering occurs when the neutrino interacts with a proton or neutron via the Z boson. This can happen with free protons or neutrons, or with individual protons or neutrons in the nuclei.



It is also possible that the neutrino “sees” the nuclei as a single particle, and not as separate nucleons, and scatters coherently.



The cross section of coherent scattering depends on A^2 , so the presence of heavy nuclei in the core greatly increases the neutrino opacity. Both free nucleon and coherent

scattering are elastic events, where the initial and final energies of the particles remain the same.

In the case of electron-neutrino scattering, the collision is inelastic as the electron cannot give up energy due to degeneracy. These scattering events cause the neutrinos to lose significant amounts of energy and leads to the thermalization of neutrinos. Electron-Neutrino scattering proceeds through the exchange of a W or Z boson. In the case of the Z boson, the muon and tau neutrinos are possible products.



Another important process in thermalizing the neutrinos is nucleon absorption and it is the inverse of neutronization.



The thermalizing of the neutrinos and their trapping in the matter reduces their luminosity by a factor of about 10^5 ergs/s [40].

As the density increases during the core collapse, these scattering and absorption events become more and more likely. Neutrinos, previously able to stream out of the core unimpeded, are now forced to undergo random walks in the matter. The material has now become partially opaque to neutrinos. When the density rises above

$$\rho_{trap} \sim 3 \times 10^{11} \frac{g}{cm^3}, \quad (3.13)$$

the neutrinos are dragged along with the matter. The timescale for the neutrinos to diffuse out of the collapsing matter approaches the timescale for the core collapse when the density reaches

$$\rho \sim 1.4 \times 10^{11} \frac{g}{cm^3}. \quad (3.14)$$

For densities above that, the timescale for neutrino diffusion is much greater than the timescale of collapse. This combined with the thermalizing of the neutrinos means that

the neutrinos do not convert enough of the gravitational potential energy, it has to take other forms, such thermal energy or bounce energy. Further research on neutrino interactions in hot and dense mediums will improve our understanding of their role in core collapse supernovae.

3.5 White Dwarfs and Chandrasekhar Limit

One of the first instances of applying statistical mechanics to astronomy was using Fermi statistics to examine the properties of white dwarf stars. Stars are a constant battle between opposing forces: the tendency of matter to gravitationally collapse and the radiative pressure produced by fusion. White dwarfs are stellar evolutionary endpoints for stars whose masses at the end of their stellar lifetime are not sufficient enough to collapse further to a neutron star or black hole [9]. White dwarfs are unusually faint, but have a color, which is normally associated with much brighter stars. Their brightness comes from the release of gravitational energy as the star slowly contracts and cools over billions to trillions of years. It is theorized that white dwarfs will eventually radiate away all of their thermal energy and become black dwarfs: cold and inert.

There are two mass regimes for white dwarf stars, high mass and low mass. Because stars experience mass-loss during the later stages of their lives, it is more useful to talk about their zero-age main sequence mass, the mass they were at when hydrogen fusion started in their core and they reached the main sequence of the HR diagram. High mass white dwarfs are those with ZAMS of 8 to $10.5 M_{\odot}$ and will fuse up to carbon in their cores before gravity overcomes the radiative pressure and causes the star to collapse into a white dwarf. High mass white dwarfs will have oxygen, neon, and magnesium in their compositions as well as helium. Low mass white dwarfs are those with ZAMS below $8M_{\odot}$ whose cores are unable to fuse carbon. They are primarily composed of helium.

Our idealized model has $mass \approx 10^{33} kg$ of helium, spherical in shape with a uniform density $\rho \approx 10^7 g/cm^3$, and central temperature of $T_c = 10^7 K$. The mean thermal energy per particle of this system is greater than the ionization energy of the helium, so we can also assume that the helium gas is completely ionized.

The mass of our system can be found by the equation

$$M \simeq N(m + 2m_p) \simeq 2Nm_p, \quad (3.15)$$

where M is the total mass, N is the number of particles, m is the mass of the electron, and m_p is the mass of the proton. Because the mass of the electron is much less than the mass of the proton, we can ignore its contribution. The factor of 2 comes from the fact that most stable isotopes of helium, carbon, and oxygen have an equal number of protons and neutrons. In our case, we are only concerned with helium, but the logic still holds [31].

The electron density is then as follows

$$n = \frac{N}{V} \simeq \frac{\frac{M}{2m_p}}{\frac{M}{\rho}} = \frac{\rho}{2m_p} \quad (3.16)$$

where V is the volume of the system and ρ is the mass density. Taking $\rho \approx 10^7 g/cm^3$, we find the electron density is on the order of 10^{30} electrons per cubic centimeter.

The Fermi momentum of an electron gas is given by

$$p_F = \left(\frac{3N}{4\pi gV} \right)^{\frac{1}{3}} h = \left(\frac{3n}{8\pi} \right)^{\frac{1}{3}} h \quad (3.17)$$

where g is a statistical weight factor and taken to be equal to 2. The Fermi momentum is of the order of $10^{-17} g \cdot cm/sec$, comparable to the characteristic momentum (mc) of an electron.

The Fermi energy of the electron gas is then

$$\varepsilon_F = \left(\frac{3N}{4\pi gV} \right)^{\frac{2}{3}} \frac{h^2}{2m} \quad (3.18)$$

and comparable to the rest energy of the electron (mc^2).

The corresponding Fermi temperature, which is given by

$$T_F = \frac{\varepsilon_F}{T}, \quad (3.19)$$

and is of the order of 10^{10}K .

It is now clear that the electrons in the system will be relativistic and the gas will almost be completely degenerate, as seen in

$$\frac{T}{T_F} = O(10^{-3}). \quad (3.20)$$

The helium nuclei do not significantly contribute to the dynamics of the system, so we can ignore them when looking at the first approximation and say the system is a gas composed solely of electrons. We can also neglect radiation for similar reasons [31].

Let us now look at the ground state properties of a degenerate Fermi gas. The number of electrons in the system is

$$N = \frac{8\pi V}{h^3} \int_0^{p_F} p^2 dp = \frac{8\pi V}{3h^3} p_F^3. \quad (3.21)$$

Rearranging for p_F yields the following

$$p_F = \left(\frac{3N}{4\pi gV} \right)^{\frac{1}{3}} h = \left(\frac{3n}{8\pi} \right)^{\frac{1}{3}} h, \quad (3.22)$$

where, we have taken $g = 2$.

The energy-momentum relation for relativistic particles is

$$\varepsilon = mc^2 \left[\left(1 + \left(\frac{p}{mc} \right)^2 \right)^{\frac{1}{2}} - 1 \right]. \quad (3.23)$$

The pressure of this electron gas is

$$P_0 = \frac{1}{3} \frac{N}{V} \langle pu \rangle_0 = \frac{8\pi}{3h^3} \int_0^{p_F} \frac{\left(\frac{p^2}{m}\right)}{\left[1 + \left(\frac{p}{mc}\right)^2\right]^{\frac{1}{2}}} p^2 dp \quad (3.24)$$

where u is the speed of a particle, given by

$$u \equiv \frac{d\varepsilon}{dp} = \frac{\left(\frac{p}{m}\right)}{\left[1 + \left(\frac{p}{mc}\right)^2\right]^{\frac{1}{2}}} \quad (3.25)$$

It is now useful to define a dimensionless variable, θ , such that

$$p = mc \sinh \theta \quad (3.26)$$

and

$$u = c \tanh \theta. \quad (3.27)$$

Now, redefining number of electrons and pressure in terms of θ , we get

$$N = \frac{8\pi V m^3 c^3}{3h^3} \sinh^3 \theta_F = \frac{8\pi V m^3 c^3}{3h^3} x^3 \quad (3.28)$$

and

$$P_0 = \frac{8\pi m^4 c^5}{3h^3} \int_0^{\theta_F} \sinh^4 \theta_F d\theta = \frac{\pi m^4 c^5}{3h^3} A(x), \quad (3.29)$$

where, $A(x)$ is given by

$$A(x) = x(x^2 + 1)^{\frac{1}{2}}(2x^3 - 3) + 3 \sinh^{-1} x \quad (3.30)$$

and

$$x = \sinh \theta_F = \frac{p_F}{mc} = \left(\frac{3n}{8\pi}\right)^{\frac{1}{3}} \left(\frac{h}{mc}\right). \quad (3.31)$$

Looking at the asymptotic expansions of $A(x)$ yields

$$A(x) = \begin{cases} \frac{8}{5}x^5 - \frac{4}{7}x^7 + \frac{1}{3}x^9 - \frac{5}{22}x^{11} + \dots & \text{for } x \ll 1 \\ 2x^4 - 2x^2 + 3\left(\ln 2x - \frac{7}{12}\right) + \frac{5}{4}x^{-2} + \dots & \text{for } x \gg 1 \end{cases} \quad (3.32)$$

We will now examine the configuration of the system in equilibrium. Without gravity, external walls would be needed to keep the electron gas at the density required for the given value of n . The gas exerts a pressure on the walls of the container and any compression or expansion of the gas will involve work being done. By assuming a spherical shape, an adiabatic change in V will result in a change in energy in the gas of

$$dE_0 = -P_0(n) dV = -P_0(R) \cdot 4\pi R^2 dR \quad (3.33)$$

Eq. (19) will still hold, but it now gives the change in kinetic energy of the gas when the size is changed. With the inclusion of gravitational potential, there is no need for walls to contain the gas. The gravitational potential is given by

$$dE_g = \left(\frac{dE_g}{dR} \right) dR = \alpha \frac{GM^2}{R^2} dR \quad (3.34)$$

where, α is a number of the order of unity whose value depends on the nature of the spatial variation inside the sphere. In equilibrium, the change in energy for an infinitesimal change in size should be equal to 0. Thus,

$$P_0(R) = \frac{\alpha}{4\pi} \frac{GM^2}{R^4} \quad (3.35)$$

and

$$P_0 = \frac{\pi m^4 c^5}{3h^3} A(x) \quad (3.36)$$

Next, we set Eqns. (21) and (22) equal to each other and solve for $A(x)$ using the following substitution

$$x = \left(\frac{3n}{8\pi} \right)^{\frac{1}{3}} \frac{h}{mc} = \left(\frac{9N}{32\pi^2} \right)^{\frac{1}{3}} \frac{(h/mc)}{R} \quad (3.37)$$

This substitution can be rewritten as

$$x = \left(\frac{9M}{64\pi^2 m_p} \right)^{\frac{1}{3}} \left(\frac{h/mc}{R} \right) = \left(\frac{9\pi M}{8m_p} \right)^{\frac{1}{3}} \left(\frac{h/mc}{R} \right) \quad (3.38)$$

by recalling Eq. (1), $A(x)$ can be written as

$$A \left(\left\{ \frac{9\pi M}{8m_p} \right\}^{\frac{1}{3}} \left(\frac{h/mc}{R} \right) \right) = \frac{3\alpha h^3}{4\pi^2 m^4 c^5} \frac{GM^2}{R^4} = 6\pi\alpha \left(\frac{h/mc}{R} \right)^3 \left(\frac{GM^2/R}{mc^2} \right) \quad (3.39)$$

$A(x)$ is known as the mass-radius relationship and contains an interesting combination of parameters. We have the mass of the star in terms of the proton mass, the radius of the star in terms of its Compton wavelength, and the gravitational energy of the star in terms of the electron rest energy; a fusion of quantum mechanics, special relativity, and gravity.

The radius of the star cannot be explicitly a function of the mass except in the extreme cases. Because our model has $mass \approx 10^{33} kg$, $m_p \approx 10^{-24} g$, and $\frac{h}{2\pi mc} \approx 10^{-11} cm$,

$A(x)$ will be set to unity when $R \approx 10^8 cm$. We can therefore look at the two extreme cases: $R \gg 10^8 cm$ and $R \ll 10^8 cm$ [31].

For $R \gg 10^8 cm$, $x \ll 1$, and then $A(x) \approx \frac{8}{5}x^5$, we have

$$R \approx \frac{3(9\pi)^{2/3}}{40\alpha} \frac{h}{2\pi} \frac{M^{-1/3}}{Gmm_p^{5/3}} \propto M^{-1/3} \quad (3.40)$$

For $R \ll 10^8 cm$, $x \gg 1$, and then $A(x) \approx 2x^4 - 2x^2$, we have

$$R \approx \frac{(9\pi)^{1/3}}{2} \frac{h}{2\pi mc} \left(\frac{M}{m_p} \right)^{1/3} \left\{ 1 - \left(\frac{M}{M_0} \right)^{2/3} \right\}^{1/2} \quad (3.41)$$

where

$$M_0 = \frac{9}{64} \left(\frac{3\pi}{\alpha^3} \right)^{1/2} \frac{(hc/2\pi G)^{3/2}}{m_p^2} \quad (3.42)$$

It can now be seen that as the mass of the white dwarf star increases, its radius will decrease. If the mass of the white dwarf exceeds M_0 , then the mass-radius relationship is no longer valid and the system is not in equilibrium anymore. This maximum mass is known as the Chandrasekhar limit and has been upheld by the observation and measurement of white dwarf star's mass. It is roughly equal to $1.44 M_{\odot}$. If a white dwarf exceeds this limit, the ground state pressure of the electron gas will not be sufficient to counteract the gravitational collapse of the matter [31].

This result was extremely important in the understanding of stellar evolution and for understanding the properties of Type 1A supernova. Type 1A supernova are thought to occur when a white dwarf is in a binary pair with another star. As the neighbor star evolves off the main sequence, its outer layers will expand while the star tries to maintain equilibrium between gravity and radiative pressure. The outer layers are now in a position where it is more gravitationally favorable to accrete onto the white dwarf than stay on the neighboring star. These outer layers are primarily composed of hydrogen, with some helium gas as well. As the white dwarf accretes matter from the binary partner, its mass is increasing. Eventually, the accreted mass will cause the white dwarf to exceed the Chandrasekhar mass limit. The matter on the surface will undergo a rapid thermonuclear reaction as it is compressed and begins fusion. The fusion rapidly releases energy and causes a massive explosion. The luminosity of Type 1A supernova are so high, that they are temporarily more luminous than the entire output of their host galaxy.

Because Type 1A supernova are so bright, relatively common, and are thought to occur from exact circumstances (exceed the Chandrasekhar mass limit), they are used as standard candles. Standard candles are objects of known brightness used to measure the distance to remote galaxies. It was through a study of distant Type 1A supernova in 1998 that researchers first saw the accelerating expansion of the universe [9].

CHAPTER IV: NEUTRON STARS

4.1 Introduction to Neutron Stars

This chapter will examine the structure and regional composition of neutron stars as well as review different types of neutron stars.

4.2 Neutron Star Structure

The exact internal structure of neutron stars is not currently well understood due to uncertainties in the properties of extremely dense matter. The densities encountered in the interior of a neutron star are above the neutron drip density, $\rho > 4.3 \times 10^{11} \text{ g/cm}^3$. Neutron drip occurs when inverse beta decay from relativistic electrons penetrate the nucleus. Neutrons then begin to fill up higher and higher energy levels, until the energy level becomes equal to the rest mass of the neutron [40]. At this point, newly created neutrons will not be stable in the nucleus and begin to “drip” out of the nucleus and form a fluid of free neutrons. As the density increases, both the amount of free neutrons present and the Fermi energy level rises, which eventually leads to all the neutrons dripping out of their nuclei.

The nature of the dense matter in the core is an open question in astrophysics. It is not known if neutron matter is the last form of degenerate matter, or if at higher densities that the quarks in the neutrons deconfine into quark matter [3]. This theoretical quark matter in the core is proposed in several equations of state, but it’s exact nature is still unknown due to the difficulty of modeling strong force interactions in matter.

4.3 Regions

The structure of neutron stars can be broken up into 4 main regions: the surface and envelope, the outer crust, the inner crust, and the core. It should be noted, however, that these regions are not hard boundaries, but rather are gradual transitions to new states

of matter, as the density increases. The densities encountered in the interior of a neutron star can exceed the density of an atomic nuclei, so detailed understanding of many-body nucleon interactions is needed to fully understand and model the interiors.

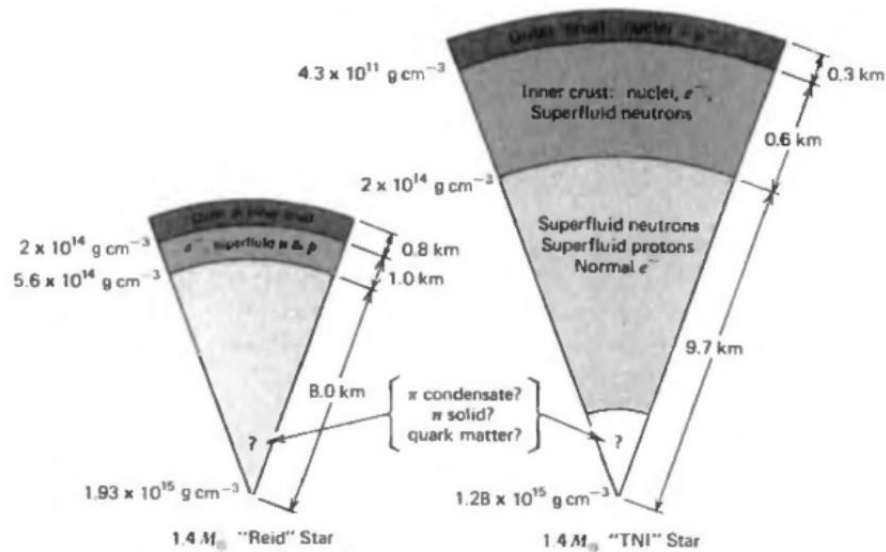


Figure 5:
Cross sectional diagram of two $1.4 M_{\odot}$ neutron stars. Reid EOS on left, TNI EOS on the right. Source [40]

Surface and Envelope

The surface and envelope of a neutron star are the least dense regions, with typical densities are below $\rho < 10^9 \text{ kg/m}^3$ (10^6 g/cm^3). They are dominated by the presence of iron-56 nuclei and non-relativistic electrons [17]. The surface and envelope do not significantly contribute to the overall mass of the neutron star since their density is orders of magnitude lower than other regions [7].

Outer Crust

The density of the outer crust is $10^{12} \text{ kg/m}^3 < \rho_{\text{Outer}} < 4 \times 10^{14} \text{ kg/m}^3$ ($10^9 \text{ g/cm}^3 < \rho_{\text{crust}} < 4 \times 10^{11} \text{ g/cm}^3$). Heavy nuclei like iron-56 is in abundance in the outer crust, but the

increasing density gives rise to relativistic electrons which can penetrate the nuclei in inverse beta-decay. This process of converting protons to neutrons in nuclei is known as neutronization and begins when the density reaches about $4 \times 10^{14} \text{ kg/m}^3$ [9].

This leads to the presence of heavier nuclei such as nickel-62, nickel-64, and so on. The heavy nuclei arrange themselves into a lattice in order to reduce the repulsive Coulomb interaction between protons in the nuclei. These heavy nuclei are stable against beta decay because there are no vacant energy levels for an emitted electron to occupy upon emission from the nuclei. The heavy nuclei are surrounded by a relativistic degenerate electron gas.

Inner Crust

The inner crust is characterized by having a density range of $4 \times 10^{14} \text{ kg/m}^3 < \rho_{\text{inner}} < 2 \times 10^{17} \text{ kg/m}^3$ ($4 \times 10^{11} \text{ g/cm}^3 < \rho < 2 \times 10^{14} \text{ g/cm}^3$). Heavy, neutron rich nuclei are still present at these densities, but begin to undergo a process known as neutron drip. When the density exceeds $4 \times 10^{14} \text{ kg/m}^3$, the minimum energy configuration for the newly created neutrons is for them to be outside the nucleus. The neutrons, in effect, drip out of the nucleus, leading to the presence of free neutrons in the inner crust.

The inner crust is composed of heavy nuclei in a lattice, relativistic free electrons, and non-relativistic neutrons. Free neutrons can spontaneously pair to form a boson, which can all occupy the same lowest energy state. Fluids composed of free neutrons are able to flow with resistance in what is known as a superfluid. Vortices in a superfluid will spin forever without losing energy [39].

When the density reaches $2 \times 10^{17} \text{ kg/m}^3 < \rho < 4 \times 10^{17} \text{ kg/m}^3$ ($2 \times 10^{14} \text{ g/cm}^3 - 4 \times 10^{14} \text{ g/cm}^3$), the nuclei will have completely dissolved into free neutrons and protons. In addition to the free neutron superfluid, the fluid of free protons also forms a superfluid and it exhibits zero electrical resistance, a property known as superconducting. The

matter at this density is fluid composed of free neutrons, free protons, and relativistic electrons. As the density increases, the amount of free protons and relativistic electrons decreases while the neutron number increases. The ratio of neutrons to protons to electrons approaches the limit of 8:1:1, as seen in the inverse beta decay correction to the Ideal, Cold n-p-e Gas model [40].

Core

The exact nature and physical makeup of the core of a neutron star is still an open question in astrophysics. The presence of superfluids in the core can lead to high surface temperatures if the superfluidity in the core cuts off the direct URCA process below the superfluid's critical temperature [34]. The densities of the core likely exceed $\rho > 4 \times 10^{17}$ kg/m³, however the exact densities in the core are model dependent so a detailed understanding of many-body nucleon interactions is needed to accurately model the core. It is possible that at such high densities and short ranges, the constituent quarks of the neutrons and protons will have their interactions weakened and experience asymptotic freedom [3]. Exotic states of matter like quark matter are not expected in neutron star's with masses less than 1.44 solar masses, but could be found in neutron star's near 2 solar masses [3]. The amount of quark matter present in the core is strongly dependent on the speed of sound in the matter, with quark cores with radii of up to 5km thought to be possible.

4.4 Types of Neutron Stars

Pulsars

Pulsars are a type of neutron star characterized by their rapid rotation and periodic emission of electromagnetic radiation along their magnetic axis. Charged particles are accelerated along field lines and strike the surface of the star, where they heat the surface. This heating causes the poles of the magnetic axis to emit broadband radio waves.

Misalignment of the magnetic axis and the rotational axis leads to the observed pulsation in the radio frequency.

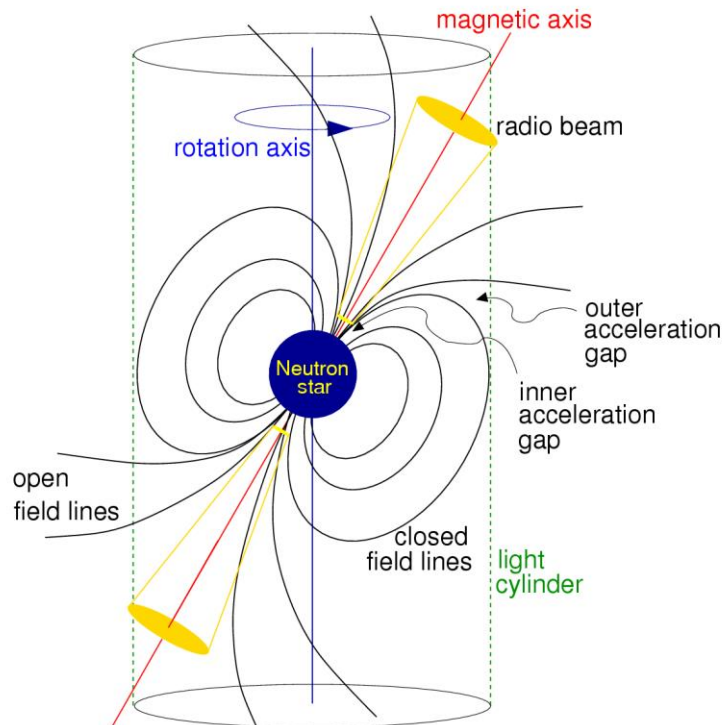


Figure 6:
Misalignment of magnetic axis and rotation axis in a pulsar, includes field lines and emission of radio beam. Source:
https://www.cv.nrao.edu/course/ast534/images/PSRs_pulsar_sketch.png

Pulsars are categorized into two main groups based on the mechanism powering their radio emission: rotation powered and accretion powered. Rotation powered pulsars generate an electric field through the movement of magnetic material. Charged particles from the surface of the star are then accelerated along these lines and strike the surface, causing the emission of the electromagnetic radiation from these hotspots. The rotation of the pulsars gradually slows over time through the release of this radiation, until the radio emissions are too weak to reach Earth or die off completely. Accretion powered pulsars

convert the gravitational potential energy of accreted matter into electromagnetic radiation. Accretion powered pulsars are found in binary systems. The binary partner star expands as it evolves and its outer layers exceed the Roche lobe. It becomes more gravitationally favorable for these outer layers to accrete onto the pulsar, which powers the pulsar's emissions. Pulsars are also classified based on their rotational period such as millisecond pulsars. However, these rotation classes can contain pulsars powered through each mechanism.

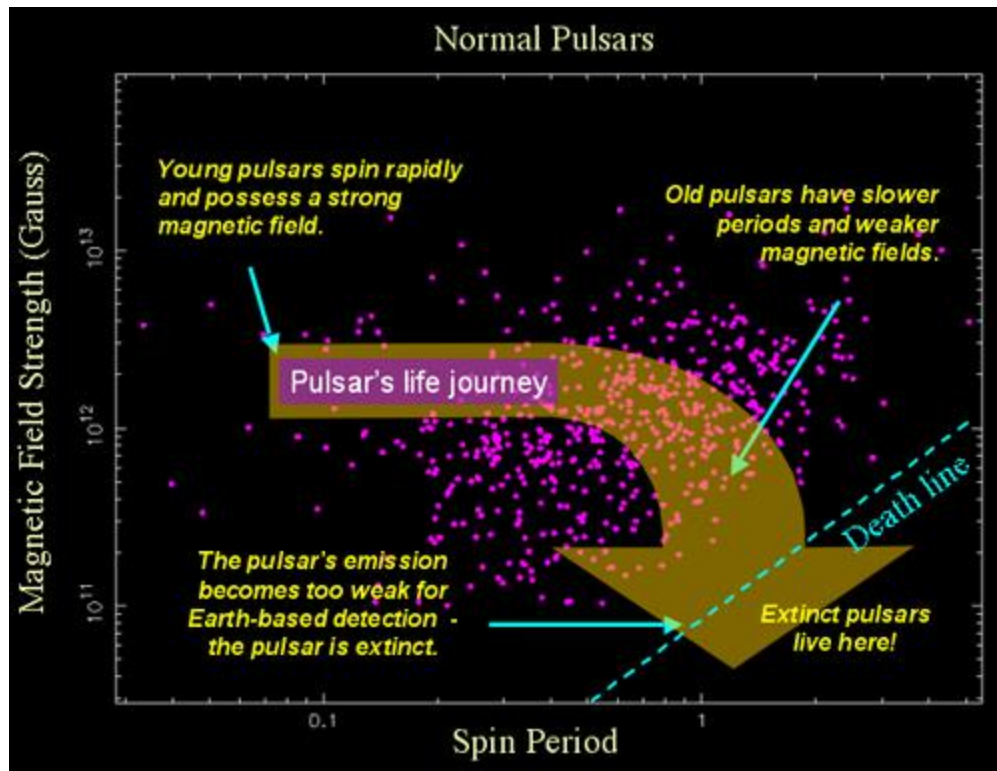


Figure 7:
 Plot of many pulsar spin periods vs magnetic field strength. Source:
<https://astronomy.swin.edu.au/cms/cpg15x/albums/userpics/pulsarevolution2.jpg>

It is possible for rotation powered pulsars to die down and be “recycled” by the evolution of their binary pair and become an accretion powered pulsar. This type of system evolution may be responsible for the millisecond pulsar [42].

Because pulsars spin down on such long timescales, their period of rotation is extremely consistent. So consistent, that many pulsars rival the accuracy of atomic clocks in terms of reliable periods. However, pulsars can experience sudden changes in their rotation rate known as glitches. These glitches are usually in the form of a decrease in the rotation rate, however increases in the rotation rate have been known to occur. One of the leading theories to explain the glitch phenomena is a possible transfer of momentum between the crust and interior superfluids. Both the crust and superfluid regions are rotating with the pulsar. However, the crust might experience deceleration caused by the pulsar's magnetic dipole radiation [17], while the superfluid is unaffected due to being weakly coupled with the surrounding matter. It is thought that glitches occur if the difference between the spin rates of the crust and superfluid become too great, leading to an internal readjustment.

Pulsar's have lots of unique properties that allow for their use as astronomical tools. As mentioned earlier, pulsar's rotation rates are incredibly consistent on our human timescale, making them very accurate clocks, with some periods of rotation being successfully measured to 13 significant digits. Their regular pulsation also allows for their use as positional reference points. The two Pioneer and two Voyager probes all carry an engraving of the Sun's position relative to 14 pulsars, each described by their unique pulsation timing.

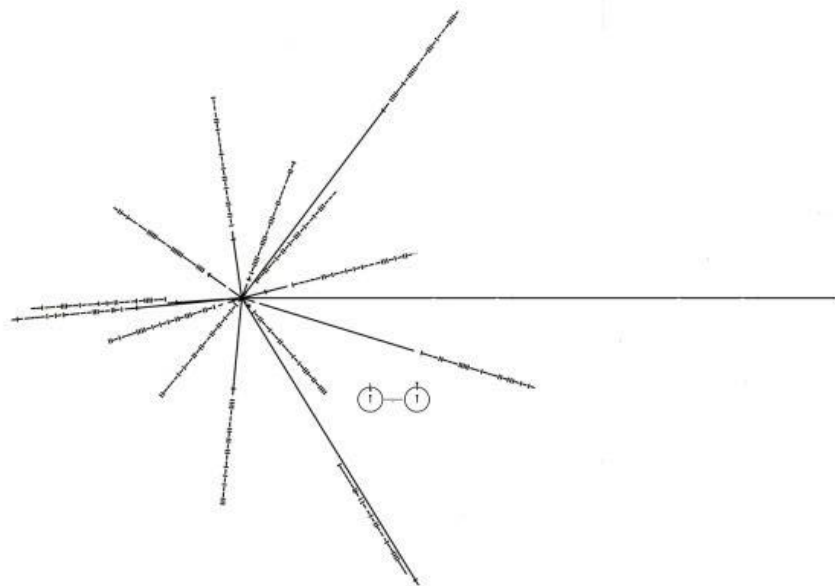


Figure 8:
Pulsar Map of the Sun's relative position engraved on Pioneer and Voyager probes.
 Source: <https://to-the-stars-web-assets.s3.amazonaws.com/files/Pulsar%20Map.jpg>

Pulsar timing has applications in gravitational wave astronomy as well. Several international groups formed the International Pulsar Timing Array (IPTA) which looks at the pulse timings for many pulsars across the sky. Any passing gravitational waves will leave a signature on the affected pulsar emissions due to the lengthening or shortening of the distance between the pulsar and the observer. The sensitivity of interferometers is based on the length of its baseline, meaning pulsar timing arrays offer baseline lengths many orders of magnitudes longer than anything possible on Earth, or in the Solar System [35].

Pulsar emissions are also a useful probe of the contents of the interstellar medium between the star and Earth. The interstellar plasma is dispersive, which causes lower frequency radio waves to travel slower than high frequency radio waves. By measuring the delay in the arrival time of the pulses, one can measure the dispersion measure, which is given by

$$DM = \int_0^D n_e(s) ds \quad (4.1)$$

where D is the distance to the pulsar and n_e is the column density of free electrons between the observer and the pulsar.

Magnetars

Magnetars are type of neutron star with magnetic field strengths on the order of 10^9 - 10^{11} Tesla (or 10^{13} - 10^{15} Gauss) [33] which is converted into very high energy electromagnetic radiation. It is thought that magnetars form when protoneutron stars have the right combination of spin, temperature, and magnetic field. This particular combination starts a dynamo process in which the thermal and rotational energy is converted into magnetic energy. It is estimated that about 1 in 10 neutron stars initially form as magnetars. Their lifetimes as a magnetar is short-lived though, as the magnetic field decays in around 10,000 years, and the star settles down as a typical neutron star.

During the lifetime of the magnetar, its massive magnetic field powers the emission of high energy electromagnetic radiation. It is thought that magnetars are responsible for the observations of soft gamma ray repeaters (SGR's), anomalous x-ray pulsars (AXP's), and fast radio bursts (FRB's) [9],[3].

Quark Stars

Quark stars are a hypothetical class of compact objects with densities above that of a neutron star, but are stable against further collapse due to quark degeneracy pressure. In the hot interiors of neutron stars, it has been theorized that the dense neutron matter deconfines into its constituent quarks, but the exact point of transition from neutron matter to quark matter is not known. High energy experiments with particle accelerators have successfully formed quark-gluon plasmas. However, the experimental quark-gluon plasma decays very quickly and is formed at temperatures higher than expected in either

neutron star cores or in quark stars. The conditions required to replicate “cold” quark matter require conditions not possible in experiments, which leads to lots of uncertainties in the exact nature of quark matter [3].

Quark matter in the cores of neutron stars and quark stars is thought to behave as a Fermi liquid and experience a color-flavor-locked (CFL) phase of color superconductivity [2]. For pure quark stars, the surface would be significantly less dense than the core, so quarks on the surface would potentially behave as a non-CFL quark liquid [2],[41]. However, no quark stars have yet been observed and are still purely hypothetical objects as such.

CHAPTER V:
EQUATIONS OF STATE AND BETA PROCESSES

5.1 Introduction to Neutron Star Equations of State

An equation of state describes the state of matter in the system while under specific physical conditions. Oppenheimer and Volkoff [27] found that the equations governing hydrostatic equilibrium for a spherically symmetric object are

$$\frac{dp}{dr} = -\frac{G(m + 4\pi r^3 p / c^2)(\epsilon + p)}{c^2 r(r - 2GM / c^2)} \quad (5.1)$$

and

$$\frac{dm}{dr} = 4\pi \frac{\epsilon}{c^2} r^2 \quad (5.2)$$

where p is the pressure, ϵ is the mass-energy density, r is the radial coordinate, and m is the mass within the enclosed sphere. These equations have boundary conditions $m(r = 0) = 0$ and $p(r = R) = 0$ where R is the radial coordinate to the surface [18]. The equation of state is given by the relation $p(\epsilon)$.

Equations of states that model the physics of neutron stars are tested by creating a series of stars with different critical densities and looking for the range of stability given by that equation of state. This stable range gives the minimum and maximum mass and radii possible for neutron stars in the given model.

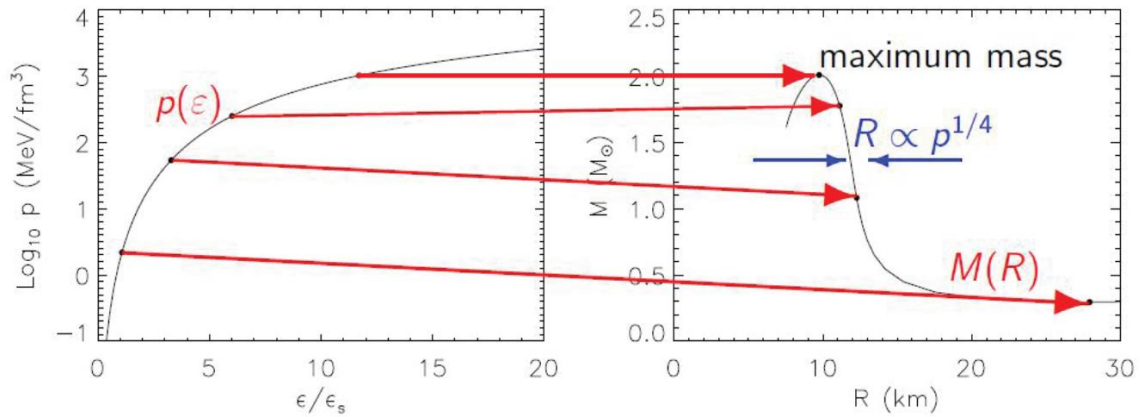


Figure 9:
 Generation of $M(R)$ curve from a specific EOS $p(\epsilon)$. $\epsilon_s \approx 150 \text{ MeV fm}^{-3}$ is the energy density at the nuclear saturation density $n_s \approx 0.16 \text{ fm}^{-3}$. Source [18].

There are basically two types of equations of state: soft and stiff. Soft equations of state will produce a small increase in pressure for an increase in density. This means that matter in a system modelled by a soft equation of state is more easily compressible and the radii of neutron stars for a soft equation of state will be smaller than their stiff counterparts. Stiff equations of state produce a much larger increase in pressure when the density is increased, and so exhibit a greater resistance to compression. This leads to the modelled neutron stars having larger radii than their soft counterparts.

Observations of neutron stars are limited to macroscopic properties such as total mass, radius, temperature, or rotational period. The equations of state should model the interior of neutron stars such that the given ranges for these properties are consistent with observations.

5.2 Observational Constraints

Observations of neutron stars provide a wealth of information, such as the star's size, mass, period of rotation, and emission spectra, that is incredibly useful for putting constraints on equations of state. These properties can then be compared to the ranges predicted by different equations of state and used to rule a model if the observed values

are outside the predicted ranges of that equation of state. Properties such as the size, period of rotation, and the profile of the emission spectra can be found for isolated and binary neutron stars, while mass estimation requires the presence of a binary partner. Since neutron stars have large temperatures, their peak wavelength falls outside the optical, but they can be very bright radio, X-Ray, and gamma ray sources and are most often studied in these wavelengths. Analysis of the emissions and the timing of pulses can give very detailed information about a single neutron star or system of neutron stars.

Mass Measurements

There are more than 2500 pulsars observed in our galaxy, mostly found as radio pulsars [28]. According to Ozel and Freire, almost 90% of all radio pulsars are isolated and so cannot have their masses measured [28]. The remaining pulsars are mostly found in binary systems, with a few exceptions found in multi-component systems. The masses of each neutron star in a binary pulsar system, where one of the pulsars is a “recycled” pulsar, can be estimated by precisely measuring the pulse timing from each pulsar. Measuring a pulse time with a precision of $1\mu s$ can give the range of the pulsar relative to the center of mass with an accuracy of 300m per measurement. This accuracy is much smaller than the size of the orbits and thus offers a uniquely precise way to obtain the Keplerian orbital parameters, and from there, the masses of the stars. Below are figures which plot the distribution of neutron star mass across different types of neutron star systems.

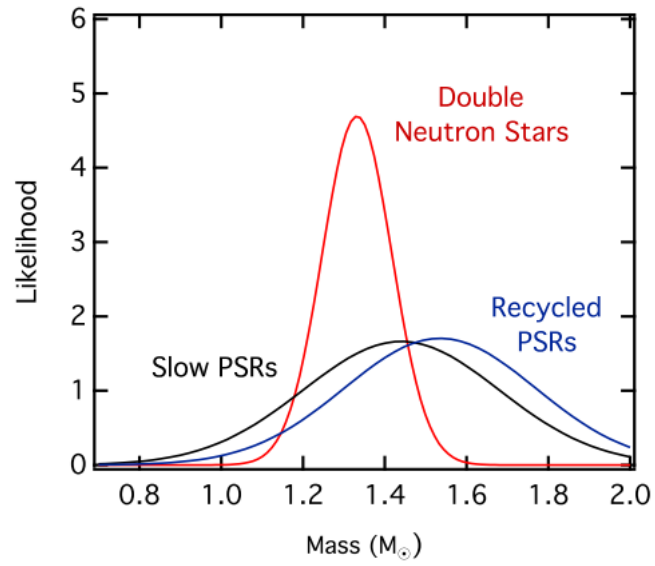


Figure 10:
Mass distribution for different populations of neutron stars. Source [28]

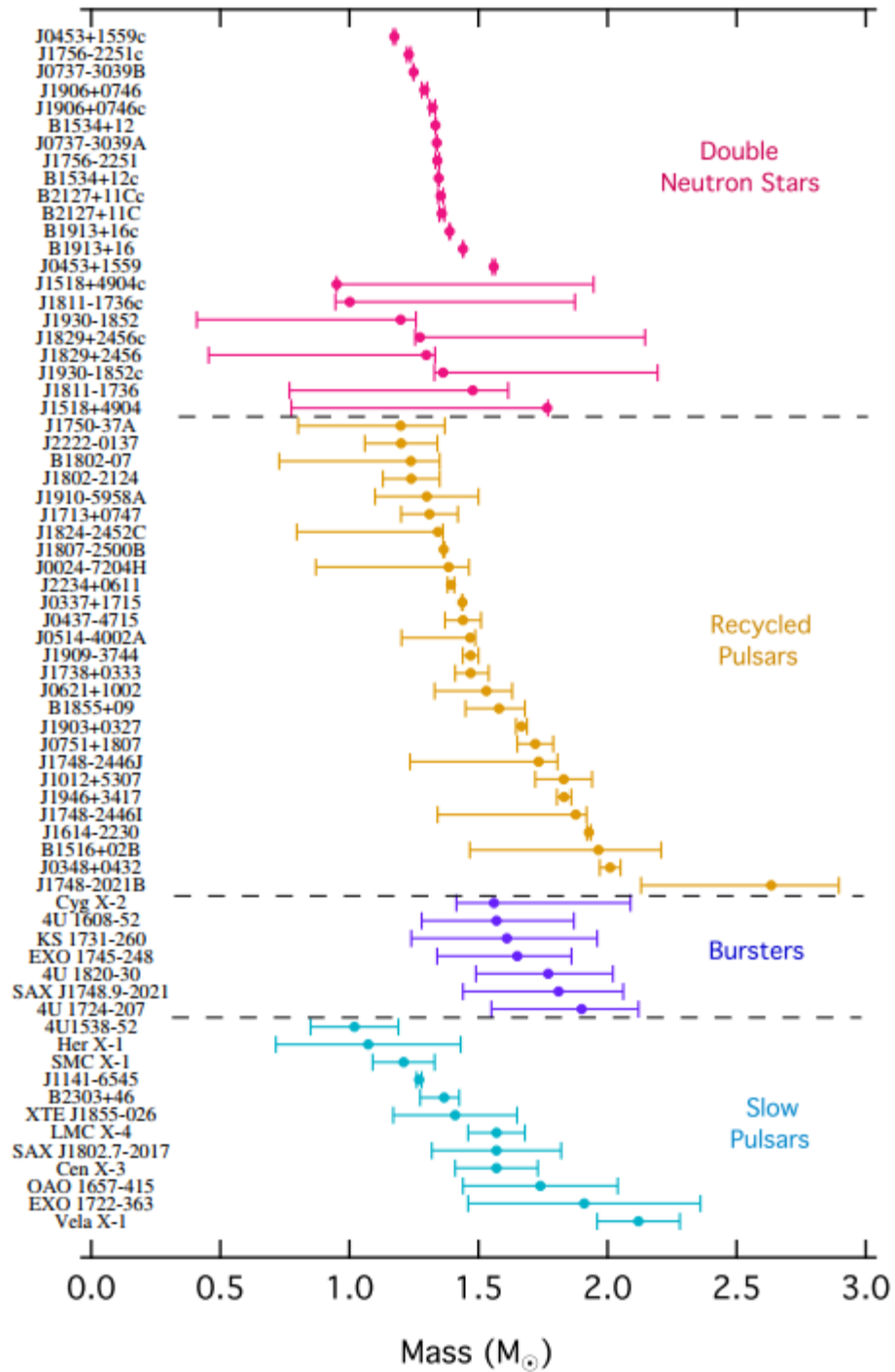


Figure 11:
Measured neutron star masses sorted by type of system. Source [28]

The end product of a supermassive special event depends on the mass, density, and the type of material. A limit on the maximum possible allowed concentration of neutrons, for neutron stars, is not well known and may represent the boundary between neutron stars and exotic forms of matter like black holes or quark stars. Gravitational wave astronomy provides a unique method to probe the allowed maximum mass by observing the mergers of massive, compact objects. Analysis of the gravitational wave event GW170817 and its observed optical counterpart, which are believed to have been generated by the merger of a binary neutron star system, led to an upper limit of $M_{max} \leq 2.17 M_{\odot}$ with 90% credibility [19]. A much more recent gravitational wave event, GW190814, is believed to have been caused by the merger of a $22.2 - 24.3 M_{\odot}$ black hole with a compact object of $2.50 - 2.67 M_{\odot}$. The exact nature of the compact object, whether it was an extremely massive neutron star, a stellar mass black hole, or something else, is unknown. It would be either the most massive neutron star or lightest black hole ever detected in a double compact-object system [1]. GW190814 is also the most uneven mass ratio detected for compact object systems. Its very formation challenges current astrophysical models of binary system formation.

Radius Measurements

The methods used to measure the radii of neutron stars can be broken up into two categories: spectroscopic and timing measurements. Both methods rely on the detection of thermal emissions from the surface to either measure the apparent angular size or to measure the spacetime effects of the neutron star on the emission itself.

Spectroscopic measurements of neutron star radii are similar to those of regular stars, but are complicated by the very compact nature of the neutron star since they gravitationally lens their own surfaces. The spectrum of the thermal flux, F , is used to

determine the effective surface temperature, T_{eff} , which are combined with the estimated distance to give an observed radius of

$$R_{\text{obs}} = D \left(\frac{F_{\text{bol}}}{\sigma_B T_{\text{eff}}} \right)^{1/2} \quad (5.3)$$

where R_{obs} is related to the physical radius by the mass dependent correction

$$R_{\text{obs}} = \left(1 - \frac{2GM}{Rc^2} \right)^{-1/2} R \quad (5.4)$$

The above relations hold for neutron stars with lower spin rates. However, high spin neutron stars cannot have their spacetime described by a Schwarzschild metric and require spin-dependent corrections to R_{obs} as well as a mass correction. It also assumes a uniform temperature distribution across the surface, which may not hold in high magnetic fields or in the case of an accreting neutron star [28]. Another source of error is accurately knowing the distance to the neutron star, something very tricky in astronomy in general. One of the more reliable methods, parallax measurements, requires that the neutron star be relatively close to the Earth. This method was used to determine the distance to a nearby cluster of neutron stars known as the Magnificent Seven [14].

Mass-Radius Relationship

Evaluating neutron star equation of states generate unique relations between the mass and radius. Neutron stars of a particular mass will have a corresponding range of radii under which the star would remain stable. Understanding the mass-radius relation would greatly benefit the study of neutron stars by placing further constraints on equations of state. Based on observations of transient accreting sources and bursting sources, Steiner, Lattimer, and Brown found that for a 1.4 solar mass neutron star, its radius would be somewhere between 10.4 and 12.9km [41].

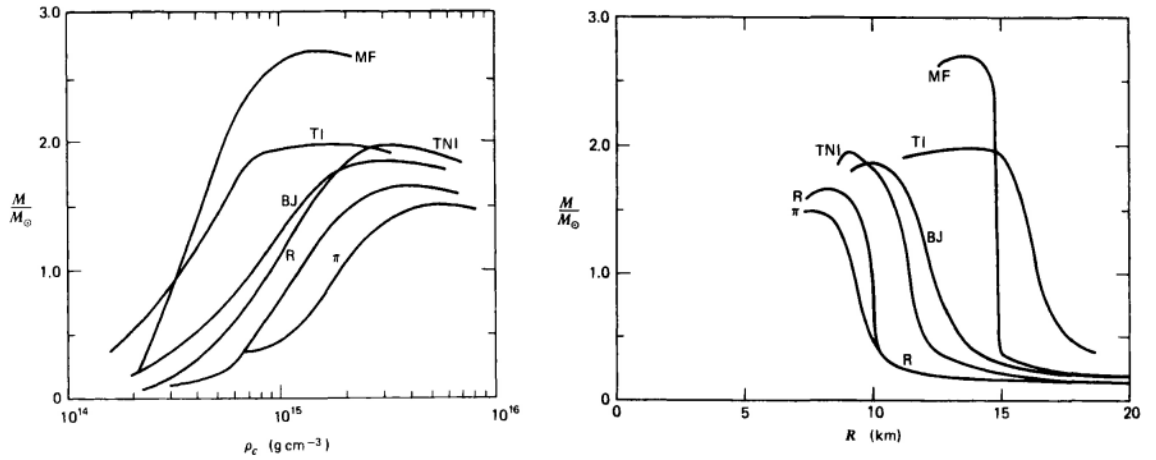


Figure 12:
 Mass-central density relation and mass-radius relation for various neutron star EOS.
 Source: [40]

5.3 Equation of State Below Neutron Drip

Ideal Cold Neutron Gas

Our discussion of equations of state for neutron stars will be most beneficial if we begin in the density regime below which much of the neutron star resides. This will give us a mathematical background for understanding both the derivation of equations of state and densities of above neutron drip can complicate our construction of an equation of state. We will also be making the same assumptions that Oppenheimer and Volkoff made in 1939 [27] and be treating the material in the neutron star as a cold ideal Fermi gas composed solely of neutrons. We know this approach to be inaccurate, but it provides a solid starting point in examining the equations of state of neutron stars.

We begin by looking at the distribution function in phase space

$$f(x, p, t) \cdot \frac{g}{h^3} = \frac{dN}{d^3x \cdot d^3p} \quad (5.5)$$

where h is Planck's constant and g is the statistical weight, the number of states available to a particle with momentum \mathbf{p} . The statistical weight is given by the equation

$$g = 2S + 1 \quad (5.6)$$

where S is the spin of the particle species. The number density for each species of particle is then given by the following equation and integrated over all momenta.

$$n = \int_{-\infty}^{\infty} \frac{dN}{d^3x \cdot d^3p} d^3p \quad (5.7)$$

The energy density of the system is then given by

$$\varepsilon = \int_0^{\infty} E \cdot \frac{dN}{d^3x \cdot d^3p} d^3p \quad (5.8)$$

where the total energy E is

$$E = \sqrt{p^2 c^2 + m^2 c^4} \quad (5.9)$$

and m is the rest mass of the particle. For a system with an isotropic distribution of momenta, the pressure P of the system is written as:

$$P = \frac{1}{3} \int_{-\infty}^{\infty} p v \cdot \frac{dN}{d^3x \cdot d^3p} d^3p \quad (5.10)$$

where the speed v is given as:

$$v = \frac{pc^2}{E} \quad (5.11)$$

The distribution function of an ideal gas in equilibrium depends on the spin statistics of the particles at energy E and is given by

$$f(E) = 1 / \left(\exp \left[\frac{(E - \mu)}{kT} \right] \pm 1 \right) \quad (5.12)$$

where μ is the chemical potential, k is Boltzmann's constant, T is the temperature of the system, and the plus sign indicates fermions, which follow Fermi-Dirac statistics, and the minus refers to bosons, which follow Bose-Einstein statistics. We are looking at a system composed overwhelmingly of fermions in the temperature domain where T is much smaller than the chemical potential for superdense systems such that $(\mu/kT \rightarrow large)$. However, just to understand the meaning of chemical potential, we set T very small and

density ignorable, such that the distribution function for completely degenerate Fermi gas then becomes

$$f(E) = \begin{cases} 1, & E \leq E_f \\ 0, & E \geq E_f \end{cases} \quad (5.13)$$

where $\mu = E_f$ is called the Fermi Energy which corresponds to the electron distribution due to its spin statistics at absolute zero temperature.

The ultimate fate of an isolated neutron star is to eventually radiate all its excess thermal energy away and reach $T = \text{ignorable}$. Even though the star will eventually reach zero temperature, there is still pressure present which is preventing the neutron star from collapsing gravitationally. The simplest equation of state is that of a cold, degenerate, single species of non-interacting fermions, and these conditions are difficult to achieve in supermassive systems. Neutron stars are not solely composed of neutrons. They are composed of a significant number protons and electrons due to inverse beta decay as well. It makes neutron stars an interacting system of oppositely charged particles, with all types of fundamental interactions at different scales. Zero temperature is not even a possibility due to the relativistic energies. The Fermi energy of this system can therefore be written as:

$$E_f = \sqrt{p_f^2 c^2 + m_n^2 c^4} \quad (5.14)$$

The number density for neutrons, ignoring the interactions with the medium are then defined as

$$n_n = \frac{2}{h^3} \int_0^{p_f} 4\pi p^2 dp = \frac{8\pi}{3h^3} p_f^3 \quad (5.15)$$

It is helpful to define a dimensionless parameter, x , which is sometimes called the relativity parameter

$$x = \frac{p_f}{m_n c} \quad (5.16)$$

For low energy, non-relativistic neutrons, $x \ll 1$. As the momentum of the neutrons increases to relativistic velocities, the parameter x will approach 1. The number density of neutrons can then be expressed in terms of x and will be a function of neutron momenta, such that

$$n_n = \frac{1}{3\pi^2 \lambda_n^3} x^3 \quad (5.17)$$

where λ_n^3 is the neutron Compton wavelength, given by

$$\lambda_n = \frac{h}{2\pi \cdot m_n c} \quad (5.18)$$

The equation for pressure due to neutrons can now be rewritten using our new definitions as

$$P_n = \frac{2}{3h^3} \int_0^{p_f} \frac{p^2 c^2}{(p^2 c^2 + m_n^2 c^4)} 4\pi p^2 dp = \frac{8\pi m_n^4 c^5}{3h^3} \int_0^x \frac{x^4}{(1+x^2)^{1/2}} dx \quad (5.19)$$

$$= \frac{m_n c^2}{\lambda_n^3} \phi(x) \quad (5.20)$$

where

$$\phi(x) = \frac{1}{8\pi^2} \left[x(1+x^2)^{1/2} \left(\frac{2x^3}{3} - 1 \right) + \ln \left[x + (1+x^2)^{1/2} \right] \right] \quad (5.21)$$

The energy density stated previously can then stated as

$$\varepsilon_n = \frac{2}{h^3} \int_0^{p_f} (p^2 c^2 + m_n^2 c^4)^{1/2} 4\pi p^2 dp$$

$$= \frac{8\pi m_n^4 c^5}{h^3} \int_0^x x^2 (x^2 + 1)^{1/2} dx \quad (5.22)$$

$$= \frac{m_n c^2}{\lambda_n^3} \chi(x) \quad (5.23)$$

where

$$\chi(x) = \frac{1}{8\pi^2} \left[x(1+x^2)^{1/2} (1+2x^2) - \ln \left[x + (1+x^2)^{1/2} \right] \right] \quad (5.24)$$

The density of the system, ρ , can be found from the equation

$$\rho = \rho_0 + \frac{\varepsilon_n}{c^2} = m_n n_n + \frac{\varepsilon_n}{c^2} = \frac{1}{3\pi^2} \frac{m_n}{\lambda_n^3} x^3 + \frac{m_n}{\lambda_n^3} \chi(x) \quad (5.25)$$

Solving for the rest mass contribution, the lowest density ρ_0 comes out to be $\rho_0 = 6.106 * 10^{15} x^3 \text{ gcm}^{-3}$. In nonrelativistic cases, ρ_0 gives the dominant contribution in the total energy of the system and is ignored in classical systems. As the Fermi velocity of the neutrons increases towards relativistic levels, the factor of x^3 in ρ_0 will begin to approach 1 and the second term will start to become significant and cannot be ignored.

An equation of state for such systems can be written in the polytropic form as

$$P = K \rho_0^\Gamma \quad (5.26)$$

where K and Γ are constants. This equation can be evaluated in two regimes, the nonrelativistic and extremely relativistic, and they are as follows:

Nonrelativistic, $\rho_0 \ll 6.106 * 10^{15} \text{ gcm}^{-3}$

$$\Gamma = \frac{5}{3}, \quad K = \frac{3^{2/3} \pi^{4/3} \hbar^2}{5 m_n^{8/3}} = 5.3802 \times 10^9 \text{ cgs} \quad (5.27)$$

Extremely relativistic, $\rho_0 \gg 6.106 * 10^{15} \text{ gcm}^{-3}$

$$\Gamma = \frac{4}{3}, \quad K = \frac{3^{1/3} \pi^{2/3} \hbar c}{4 m_n^{4/3}} = 1.2293 \times 10^{15} \text{ cgs} \quad (5.28)$$

5.4 Inverse Beta Decay Correction to EOS

The previous discussion relied on the assumption that the gas was composed solely of neutrons, so we will now look at the case where the gas is also composed of electrons and protons. As previously discussed, at high densities, the electrons become relativistic and acquire enough energy to penetrate the nucleus. This reaction, known as inverse beta decay, is one of the most important corrections in constructing an equation of state for a neutron star.

$$e^{-} + p \rightarrow n + \nu_e \quad (5.29)$$

For now and for simplicity's sake, we will assume the neutrinos generated in the above reaction escape from the system. In order for inverse beta decay to occur, the electron must have enough energy to balance the mass difference of the proton and neutron.

$$e_{\Delta} = e_n - e_p = (m_n - m_p) c^2 \quad (5.30)$$

This energy difference is 1.29 MeV [40].

Inverse beta decay is only effective at converting electrons and protons into neutrons if normal beta decay is blocked.

$$n \rightarrow p + e^{-} + \bar{\nu} \quad (5.31)$$

This blockage can occur if the energy levels of the free electrons are filled up to the level that the electron emitted from beta decay would try to occupy. Because the highest occupied energy level is related to the density of the system, there exists a critical density such that beta decay is blocked and inverse beta decay can proceed uninterrupted.

First, let us look at the properties that a gas composed free electrons, protons, and neutrons has while in equilibrium. When this mixture is equilibrium, the chemical potential of the species will be

$$\mu_n = \mu_e + \mu_p. \quad (5.32)$$

We set the chemical potential of the neutrinos to zero since we earlier made the assumption all the neutrinos will leave the system. This would mean the number density of the neutrinos is also zero.

Expanding our definition of the relativity parameter of the neutron, x_n , from the previous section to include the proton and electron gives

$$x_n = \frac{p_F^n}{m_n c}, \quad x_e = \frac{p_F^e}{m_e c}, \quad x_p = \frac{p_F^p}{m_p c}. \quad (5.33)$$

The chemical potential of each species can then be rewritten in terms of their corresponding Fermi Energy,

$$\mu_i = \left[(p_{Fc}^i)^2 + (m_i c^2)^2 \right]^{\frac{1}{2}} \quad (5.34)$$

so that Eq. (5.32) can be rewritten as

$$m_e (1 + x_e^2)^{1/2} + m_p (1 + x_p^2)^{1/2} = m_n (1 + x_n^2)^{1/2}. \quad (5.35)$$

By assuming charge neutrality, we can put limitations on the number of protons and electrons in our system.

$$n_e = n_p \quad (5.36)$$

Recalling Eq. (5.13) for number of particles of a species in terms of its relativity parameter and applying charge neutrality, we arrive at

$$\frac{1}{3\pi^2 \lambda_e^3} x_e^3 = \frac{1}{3\pi^2 \lambda_p^3} x_p^3, \quad (5.37)$$

which is equivalent to

$$m_e x_e = m_p x_p. \quad (5.38)$$

One can then determine the equation of state for this system in terms of the relativity parameter of the electron, x_e . Start by choosing a value for x_e , solving Eq. (5.37) for x_p , and then solving Eq. (5.35) for x_n . The pressure, average energy per particle, and total number of particles can then be found using Eq. (5.19-5.25). The pressure and average energy per particle are simply the sum of each species contribution.

$$P = \frac{m_e c^2}{\lambda_e^3} \phi(x_e) + \frac{m_p c^2}{\lambda_p^3} \phi(x_p) + \frac{m_n c^2}{\lambda_n^3} \phi(x_n) \quad (5.39)$$

$$\varepsilon = \frac{m_e c^2}{\lambda_e^3} \chi(x_e) + \frac{m_p c^2}{\lambda_p^3} \chi(x_p) + \frac{m_n c^2}{\lambda_n^3} \chi(x_n) \quad (5.40)$$

$$n = \frac{1}{3\pi^2\lambda_p^3}x_p^3 + \frac{1}{3\pi^2\lambda_n^3}x_n^3 \quad (5.41)$$

The minimum density where neutrons begin appearing in the gas can be found by setting $x_n = 0$ in Eq. (5.35). It will turn out that protons in this density are nonrelativistic and so we have $x_p \ll 1$. We will define a variable Q in terms of the masses of the neutron and proton, such that

$$Q = m_n - m_p = m_e(1 + x_e^2)^{1/2}. \quad (5.42)$$

Solving for x_e in Eq. (5.33) and (5.37), we arrive at

$$n = \frac{1}{3\pi^2\lambda_e^3} \left[\left(\frac{Q}{m_e} \right)^2 - 1 \right]^{3/2} = 7.37 \times 10^{30} \text{ cm}^{-3} \quad (5.43)$$

which corresponds to a density of about

$$\rho_0 \approx nm_p \approx 1.2 \times 10^7 \text{ gcm}^{-3}. \quad (5.44)$$

So below this density, the composition is purely electrons and protons. Above this density, the proportion of neutrons increases with the increasing density. The composition can be found by substituting Eq. (5.38) into Eq. (5.35) such that

$$(m_e^2 + m_p^2 x_p^2)^{1/2} + m_p(1 + x_p^2)^{1/2} = m_n(1 + x_n^2)^{1/2}. \quad (5.45)$$

This is then squared twice and simplified to give

$$4m_n^2 m_p^2 x_p^2 (1 + x_n^2) = (Q^2 - m_e^2) \left[(m_n + m_p)^2 - m_e^2 \right] + 2m_n^2 x_n^2 (m_n^2 - m_p^2 - m_e^2) + m_n^4 x_n^4. \quad (5.46)$$

Rearranging and recalling Eq. (5.37) and (5.38) yields

$$\frac{n_p}{n_n} = \left(\frac{m_p x_p}{m_n x_n} \right)^3 = \frac{1}{8} \left[\frac{1 + \frac{2(m_n^2 - m_p^2 - m_e^2)}{m_n^2 x_n^2} + \frac{(Q^2 - m_e^2) [(m_n + m_p)^2 - m_e^2]}{m_n^4 x_n^4}}{1 + \frac{1}{x_n^2}} \right]^{3/2} \quad (5.47)$$

Because Q and m_e are both much less than m_n , so the above equation can be rewritten as

$$\frac{n_p}{n_n} \simeq \frac{1}{8} \left[\frac{1 + \frac{4Q}{m_n x_n^2} + \frac{4(Q^2 - m_e^2)}{m_n^2 x_n^4}}{1 + \frac{1}{x_n^2}} \right]^{3/2}. \quad (5.48)$$

We find that the proton-neutron ratio decreases as the density increases and reaches a minimum value at

$$\left(\frac{n_p}{n_n} \right)_{min} = \left[\frac{Q}{m_n} + \frac{(Q^2 - m_e^2)^{1/2}}{m_n} \right]^{3/2} = 0.0026 \quad (5.49)$$

when the number of neutrons is

$$n_n = \frac{2^{3/2}}{3\pi^2 \lambda_n^3} \left(\frac{Q^2 - m_e^2}{m_n^2} \right)^{3/4} \quad (5.50)$$

and the density is about

$$\rho_0 \approx m_n n_n \approx 7.8 \times 10^{11} \text{ gcm}^{-3}. \quad (5.51)$$

From this minimum, the ratio of protons to neutrons rises monotonically to $\frac{1}{8}$ as either x_n or ρ_0 approach infinity. It is in these highly dense systems that our understanding of particle interactions and the system's corresponding equations of state get more difficult to work with. Physicists have a good understanding of the equations of state for cold, dense matter when the matter is below the density known as neutron drip, or

$$\rho_{drip} \approx 4 \times 10^{11} \text{ gcm}^{-3}. \quad (5.52)$$

5.5 Thermal Evolution of Neutron Stars

Neutron stars are dynamic systems, which undergo through several stages during its evolution. Statistical conditions are associated with different stages and the local

behavior of matter depends on the chemical composition that is managed by the particle processes in the local statistical conditions. The most dominant local processes occurring in the nuclear matter are based on weak and strong processes. We incorporate the effect of quantum statistical background to these processes to understand the dynamics of star, in detail at various stages of its development.

URCA Process and Protoneutron Stars

After the supernova explosion blasts off the outer layers, the hot, dense core is all that remains. This marks the beginning of the neutron star's lifetime. The young neutron star, or protoneutron star, is exceedingly hot, with temperatures on the order of 10^{11} to 10^{12} kelvin [40]. We saw that during the core collapse, neutron decay and electron capture generated massive amounts of neutrinos which carried energy out of the system and contributed to the supernova explosion through the neutrinosphere reheating the infalling layers [6].

The protoneutron star also experiences rapid energy loss to escaping neutrinos through these same processes [34]. During the first several days of the protoneutron star, its high temperature allows weak neutron decay and electron capture process that rapidly cool the star down to 10^9 K through the energy taken out of the star by neutrinos.



However, when these processes are occurring in a protoneutron star, they are collectively known as the URCA process. It was named by George Gamow and Mario Schenberg after a casino, Cassino da Urca, notorious for quickly bankrupting its gamblers [25]. Just as the URCA casino rapidly drains the financial reserves of its gamblers, the URCA process quickly drains the energy reserves of the protoneutron star. The URCA

process is also important for determining the beta equilibrium composition of the neutron star matter.

Modified URCA Process

When the temperature drops to around 10^9K , the nucleons become degenerate as any emitted electrons would not have the energy required to fill the next available energy level. This highly suppresses the URCA reactions. It is no longer possible for the reactions to conserve both energy and momentum. Chiu and Salpeter proposed a modified version of the URCA process that relied upon the presence of a bystander particle to absorb the additional momentum [40]. The Modified URCA processes are given by



Both the URCA and Modified URCA processes are sensitive to the conditions of beta equilibrium, given by

$$\mu_e + \mu_p = \mu_n, \quad (5.57)$$

where

$$\frac{\partial \varepsilon}{\partial n_e} + \frac{\partial \varepsilon}{\partial n_p} = \frac{\partial \varepsilon}{\partial n_n}. \quad (5.58)$$

When matter is in a state of beta equilibrium, neutron decay and electron capture happen at the same rate. If the matter is not in beta-equilibrium, it will tend to attain beta equilibrium. There, certain reactions will proceed more rapidly than the other until the fractions of neutrons, protons, and electrons are once again in equilibrium.

CHAPTER VI:

EXAMINING BETA PROCESSES THROUGH QED IN HOT AND DENSE MEDIUM

When particles are in sufficiently hot and dense environments, their physical properties can be modified by their interactions with their surroundings. Quantum electrodynamics (QED) is a relativistic quantum field theory in which particles interact with fields through the exchange of virtual particles. The effect of these interactions only become apparent in sufficiently hot and dense environments. These self-interactions may introduce infinities in calculated quantities that need to be removed. Renormalization is a technique that accounts for these interactions and infinities and allows one to accurately calculate the observed properties.

Renormalization of QED at finite temperature and densities indicate that the parameters of QED are modified in an interacting medium of electrons at high temperatures and densities. Several authors have calculated QED parameters in the interacting media in different ranges of temperatures. Masood has calculated all the QED parameters in terms of generalized functions, a, b, c, \dots for all statistical contributions, depending on different ranges of temperatures and densities [20]. We use the integral form of Masood's generalized functions to calculate the number density of electrons in an interacting fluid.

Masood's functions are used to calculate electron mass, wavefunction and charge of electron and are used to describe the electromagnetic properties of QED system at extremely high temperature and densities. It is shown that the renormalization process of QED, incorporates Fermi-Dirac distribution of electron and Bose-Einstein distribution of photons contribute temperature and chemical potential dependence to all the measurable parameters of the theory. Using this renormalization scheme, electron mass, wavefunction and charge can all be expressed in terms of Masood's functions and

evaluated for different ranges of temperature and chemical potential [21]. The highest thermal contributions comes in terms of quadratic dependence of temperature and highest density dependence appears as quadratic chemical potential dependence.

Electrons in sufficiently hot and dense surroundings have their mass and charge modified by their interactions with the hot and dense background. Masood has calculated the QED thermal and density corrections for electron mass and charge. The renormalized electron mass is given by

$$m_R = m_0 + \delta m \quad (6.1)$$

where

$$\frac{\delta m}{m}(T, \mu) \approx \frac{\alpha \pi T^2}{3m^2} \left[1 - \frac{6}{\pi^2} c(m\beta, \mu) \right] + \frac{2\alpha}{\pi} \frac{T}{m} a(m\beta, \mu) - \frac{3\alpha}{\pi} b(m\beta, \mu). \quad (6.2)$$

The renormalized electron charge is given by

$$e_R = e_0 + \delta e \quad (6.3)$$

where

$$\frac{\delta e}{e}(T, \mu) \approx (Z_3(T, \mu)) - \frac{1}{2} \approx 1 + \frac{\alpha T^2}{6m^2} \left[\frac{ma(m\beta, \mu)}{T} - c(m\beta, \mu) + \frac{1}{4} \left(m^2 + \frac{\omega^2}{3} b(m\beta, \mu) \right) \right]. \quad (6.4)$$

Density and temperature contributions come through the Masood a,b,c,... functions in Eq. (6.2) and Eq. (6.4).

This change in the electron mass modifies the rate at which beta processes like electron capture and beta decay will take place, and therefore, alters the beta-equilibrium composition of neutron stars at various chemical potentials and temperatures.

Modifying the properties of the electron will also effect the propagation of photons in this hot and dense medium. This may have significant implications for both the composition and structure of neutron stars as well as their thermal evolution, as both are highly sensitive to the rates of beta decay and inverse beta decay. In order to better understand the effects described, we examine the number density of electrons across all energy levels for ranges of chemical potential and temperature.

6.1 Introduction to equations

From chapters 4 and 5, on the thermal evolution of neutron stars and the inverse beta decay correction to the ideal, cold n-p-e gas, we can see the importance of the properties of the electron in determining both the composition and structure of the neutron star.

In these calculations, we consider the background to be composed of relativistic particles which can virtually produce and interact with the medium. Relativistic energies allow us to ignore higher order terms in the power series of m/E [22]. We choose the electron, proton, neutron, and three standard neutrino flavors as our fermions and their antiparticles. All the calculations are done in CP symmetric background and taking chemical potential of antiparticles are equal and opposite to the chemical potential of the corresponding particles. We also use natural units, $c = h = k = 1$, such that $\beta = 1/T$. The fermion distribution can be further written as

$$n_f(E, \pm \mu) = \frac{1}{e^{\beta(E \pm \mu)} + 1} = \sum_{n=1}^{\infty} (-1)^n e^{-n\beta(E \pm \mu)} \quad (6.5)$$

where n_f^+ represents the particle distribution function and n_f^- represents the antiparticle distribution. We are interested in the electron, so we will look at n_f^+ . Electrons obey Fermi statistics, which limits the occupancy of each state to a single electron. Two electrons can occupy almost the same energy state as a pair of spin up and spin down particles. The energy of the electron in a constant magnetic field B is given by [7]

$$E^2 = p^2 + m_e^2 + eB(2n + 1). \quad (6.6)$$

The contribution of the last term can be ignored for small magnetic fields. However, in the presence of the high magnetic fields of neutron stars, this contribution cannot be ignored.

Due to the Fermi statistics, the number density of Fermi gas of electrons will depend on the temperature and density of the system, as the interacting fluid will not follow the free particle distribution with fixed number 2. The number density of electrons, n_e , can be calculated by integrating Eq. (6.5) over all possible energies.

$$n_e = \int n_f^+ dE = \int \sum_{n=1} (-1)^n e^{-n\beta(E \pm \mu)} dE \quad (6.7)$$

This is a number density for all possible energies of electrons while they obey Fermi-statistics. It describes the maximum occupancy of electrons per unit volume for a given temperature and chemical potential range. In the limit that $E > \mu$, such as in a very hot environment where the electrons are highly relativistic, but chemical potential is not ignorable, the distribution function n_e comes out to be [21]

$$n_e = \sum_{n=1} (-1)^{n+1} \frac{T}{n} e^{-n\mu\beta} . \quad (6.8)$$

This situation is more relevant in the early universe where $T \gg \mu$ and does not appear in any calculation in this paper explicitly because this scenario is not found in stars. Temperature dependence of QED parameters has been calculated extensively in literature and have been applied to above the nucleosynthesis temperatures [21]. We use Eq. (6.8) to calculate the maximum number of electrons per unit volume of hot and dense systems in neutron stars at different stages of evolution when chemical potential competes with temperature. We used different ranges of temperatures and chemical potentials corresponding to particular stages of a neutron star's thermal evolution. The range of chemical potentials also corresponds to different densities and nuclear environments encountered in the interior of a neutron star.

Because of the local nature of QED and field theory, the number density of electrons being discussed represent tiny regions of a large system, where only the

extremely small localities allow for the chemical potential to remain constant and dealt quantum mechanically. These pockets can occur in any region of the neutron star since the composition is not uniform. Even singular regions like the crust or outer core will have internal variations in chemical potential. However, pockets of high chemical potential will occur more frequently in denser regions while pockets of lower chemical potential will be more common in less dense regions. However, chemical potential is an indirect measure for density. Change in volume for a given mass has a direct impact on density so the effect of volume on the chemical potential of an electron gas was investigated in [44]. Williams and Goto found that an increase in volume was generally associated with a decrease in the chemical potential. Stiff equations of state that predict smaller volumes and higher densities correspond to higher chemical potentials than soft equations of state.

6.2 Evaluating and Discussing the Number Density

The average number density of electrons was determined using an original python script for a range of temperatures and chemical potentials. The temperatures were chosen to represent significant stages during the neutron star's thermal evolution, with additional temperatures chosen to give further insight on the transition between stages. These temperatures also represent the variation in temperature within the interior of the neutron star. It is thought that the core rarely exceeds temperatures of 100MeV [34].

Stage of Neutron Star Evolution	Temperature (K)	Temperature (MeV)
Beginning of Core Collapse	5×10^9	0.430866
Protoneutron Star (Upper limit)	10^{12}	86.173281
Protoneutron Star 2 (Realistic)	10^{11}	8.617328
One Day Old	10^9	0.086173
Few Hundred Years	10^8	0.008617

*Table 2:
Temperatures in Kelvin and MeV for stages of neutron star evolution*

The chemical potentials selected represent the chemical potentials encountered in different regions of the neutron star and range from $\mu = 1 \times 10^{-6} \text{ MeV}$ to $\mu = 350 \text{ MeV}$. Large chemical potentials like $\mu = 350 \text{ MeV}$ may occur in the ultra-high densities of the core predicted by some EOS, such as the relativistic Bruckner-Hartee-Fock model [43]. The very low values of chemical potential like $\mu = 1 \times 10^{-6} \text{ MeV}$ were used to investigate the least dense regions.

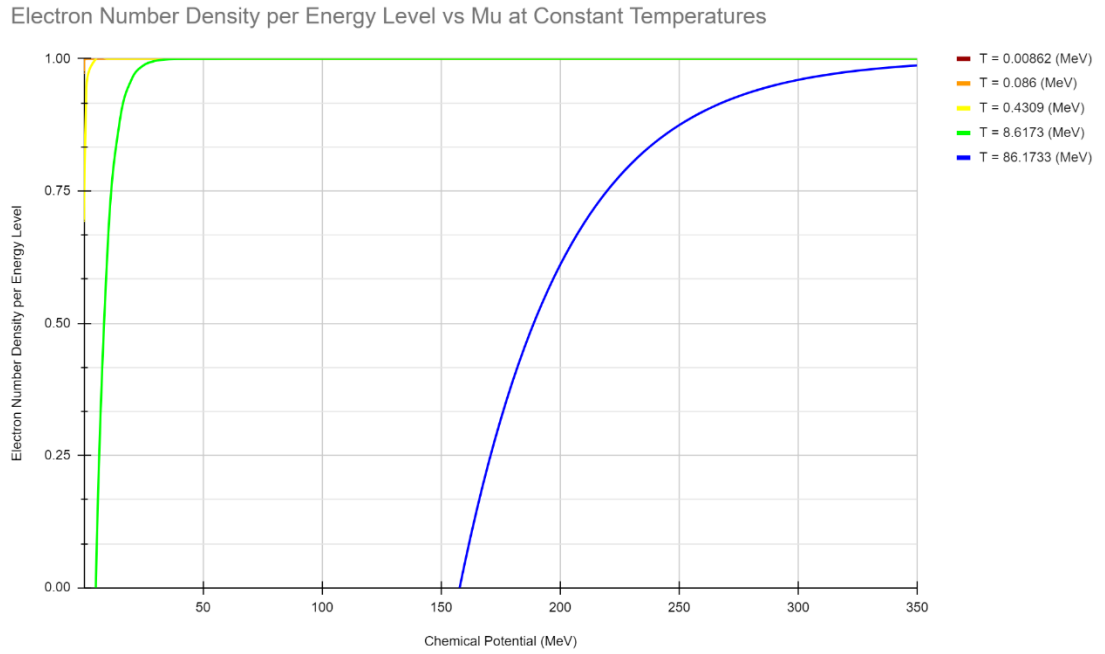


Figure 13:
Electron number densities for defined chemical potential range and temperatures from Table 1.

Figure 13 gives the electron number density with temperature. It is seen clearly that for ignorable chemical potential, the maximum value of the number of electrons in a state can only reach to unity or it can occupy all available states using Fermi-Dirac distribution and Hund's rule.

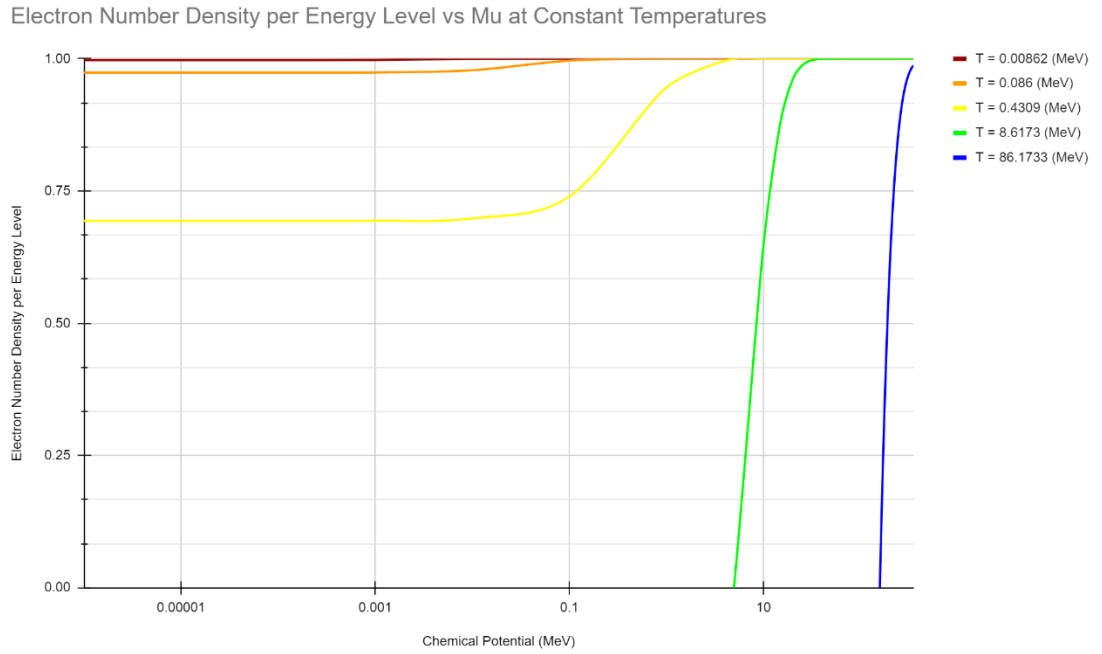


Figure 14:
Electron number densities for defined chemical potential range and temperatures from Table 1 with logarithmic scale on chemical potential

Figure 14, however shows the variation of electron number density with the chemical potential for constant temperatures. Here the chemical potential is comparable with the temperature. However, this study does not correspond to any stable physical system. This situation only occurs during the lifecycle of a star for a short period during cooling and is unstable. It occurs so quickly and is associated with the phase transition and does not allow one to create a model of the neutron star at that time during this transitory phase.

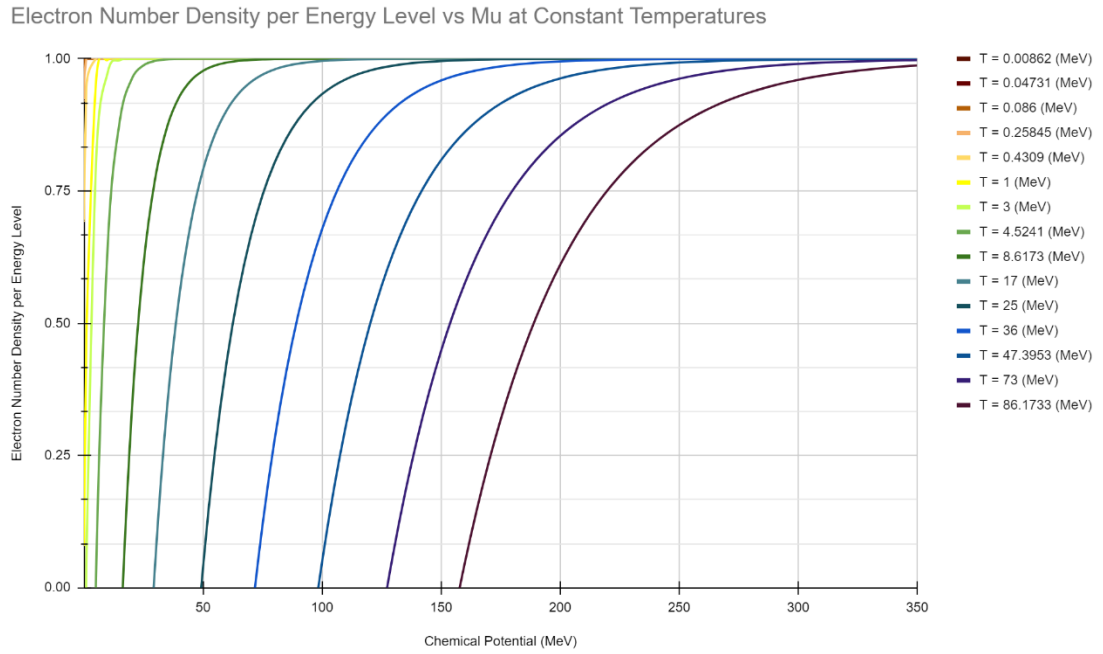


Figure 15:
Graph of n_e vs μ at constant temperatures for an expanded range of temperatures

Figure 15 includes more temperatures to further examine the behavior of number density as temperature changes. As the temperature increases, the range of positive n_e 's shrinks. This may mean low electron chemical potentials are not physically possible in such hot systems or are unstable and shortlived.

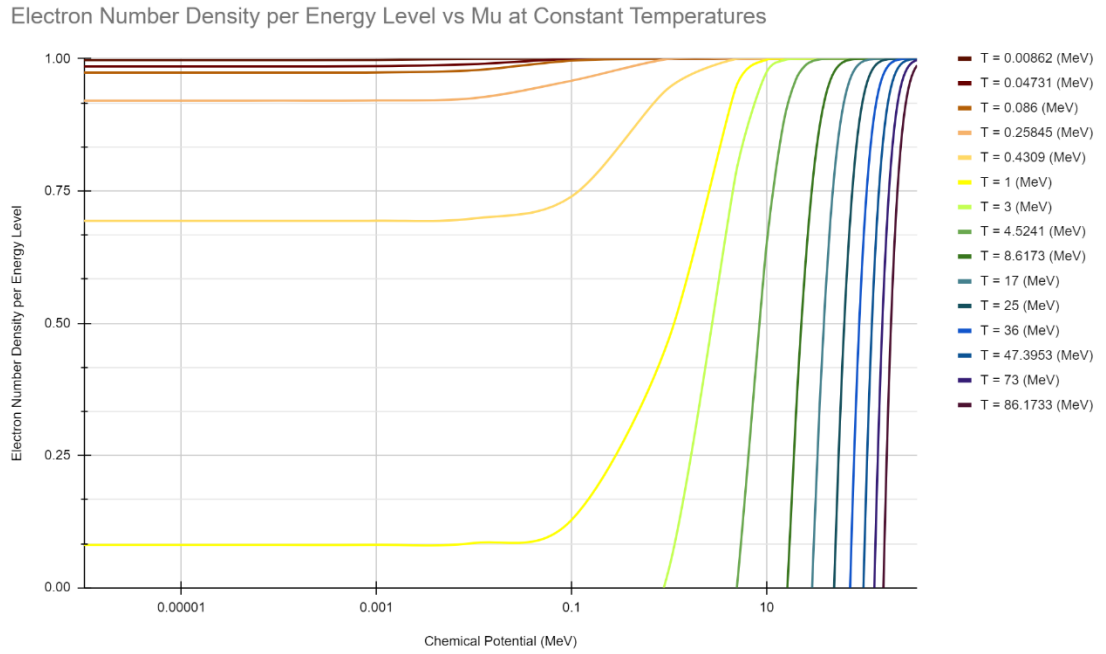


Figure 16:
Graph of n_e vs μ for constant temperatures with log scale on chemical potential for expanded temperatures

Figure 16 shows the behavior of the number density when the chemical potential becomes comparable with the temperature. As discussed for Figure 14, these situations would be unstable and only occur briefly. We see that $n_e > 0$ when the temperature decreases to $T = 1 \text{ MeV}$, this may mean regions of low chemical potential become stable around there as the temperature lowers.

Electron Number Density per Energy Level vs Mu at Constant Temperatures

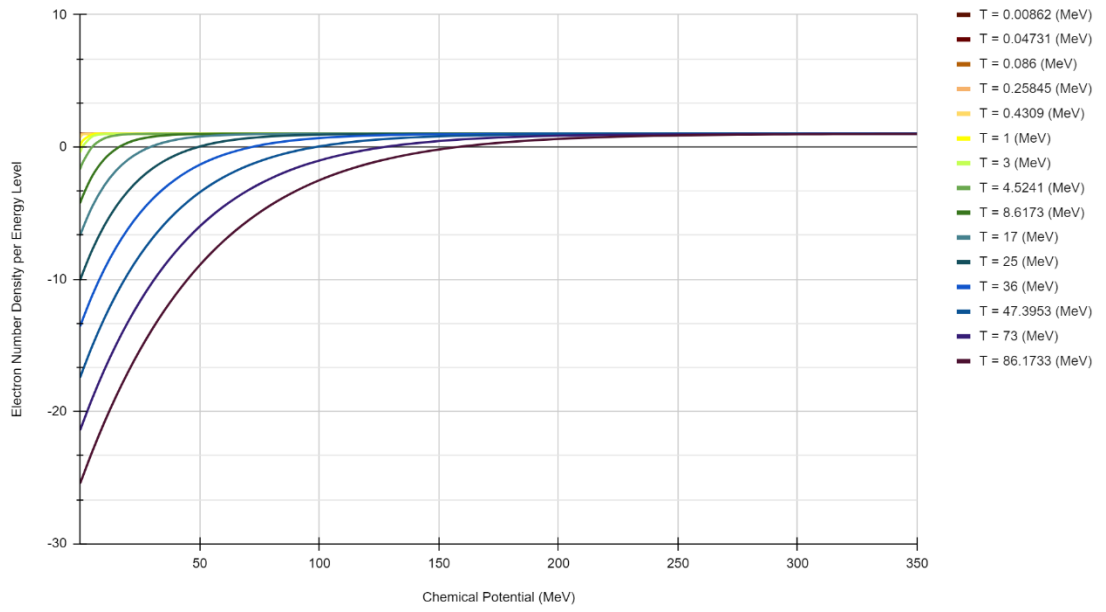


Figure 17:
Graph of n_e vs μ for constant temperatures with negative n_e values included

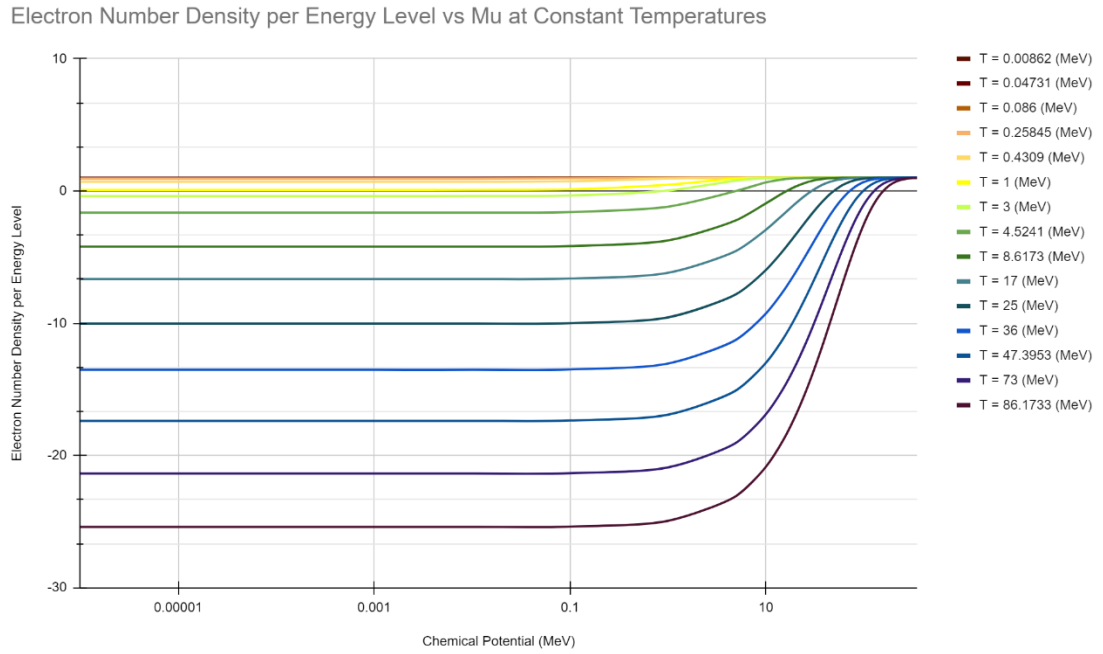


Figure 18:
Graph of n_e vs μ for constant temperatures with log scale on chemical potential and negative n_e values included

Figures 17 and 18 show the full range of number density, n_e , for the evaluated temperatures and chemical potentials. For high temperature regions where T is comparable to μ , n_e stays positive. But as $T \gg \mu$, the number density n_e takes on negative values. These negative values represent the inability of a system at that chemical potential to retain the highly energetic electrons

Discussions and Conclusions

The behavior of the n_e can be understood in the context of neutron star thermal evolution and the beta processes. Because n_e was calculated from the integration of the Fermi-Dirac distribution over all possible energies, a value of $n_e = 1$ corresponds to every possible electron energy level being filled at that temperature and chemical potential. If all the electron energy levels are occupied, neutrons are blocked from decaying since the emitted electron would have to occupy the highest possible energy

level. When $n_e \neq 1$, it means there are unfilled electron energy levels at that chemical potential and temperature. These open energy levels will allow neutron decay to proceed as the emitted electron will be able to occupy one of the open levels. As the temperature of the electron gas lowers, there are less energy levels available to the electrons, and so neutron decay begins to be suppressed.

The value of n_e also indirectly describes the rate of neutrino emission. Chemical potential is the amount of energy required to change the particle number. During beta processes, in order to conserve the lepton number, there must be an emitted neutrino or antineutrino. For low temperatures, $n_e = 1$ for nearly all chemical potentials, which is what we would expect if the rate of neutrino emission had significantly been decreased.

When $n_e < 1$, neutrons at that temperature will be able to decay into a proton, electron, and an anti electron neutrino. The electron and proton remain in the star while the antineutrino can leave the star, carrying away energy and cooling the star. The addition of the electron and proton change the conditions of beta equilibrium and may allow for them to interact with other free fermions and form a neutron through electron capture by a proton. If $n_e < 0$, this may represent regions that are not physically possible or are not stable. A negative number density implies that electrons in that temperature and chemical potential would be ejected from such a system. As temperature decreases, $n_e > 0$ for lower chemical potentials. This may mean that regions of lower chemical potential become stable as the star cools.

In the high temperature domain, like when the neutron star is younger or deeper inside an older neutron star, $T > 25 \text{ MeV}$, and $n_e < 1$ for all possible chemical potentials. This represents the regions where neutron decay and electron capture can proceed quickly. When $T = 0.086 \text{ MeV}$, $n_e \approx 1$ for all possible chemical potentials and represents the electron gas becoming degenerate. When the electron gas is degenerate, the

URCA process is suppressed and the neutron star must cool through other means like the Modified URCA process, which proceed at a much slower rate [40]. Using the value of n_e as an indicator of neutrino emission from beta processes, we see it is dominant where the temperature is higher, such as deep in the interior or closer to the surface when the neutron star is very young. As the star cools, neutrino emission from the surface would decrease and mostly come from deeper regions within the star. The behavior of n_e in both the high and low temperature domain agrees with our understanding of neutron star cooling.

6.3 Future Work

In order to continue this project, the next step would be to apply this electron number density to an equation of state, such as the cold n-p-e model and examine its effect on the mass-radius relation. Modifications to the electron properties like mass would also have an effect on the equations of state, particularly those that describe denser matter, such densities above neutron drip. Analysis into the effect of the modified properties on the rates of the various reactions should also yield valuable insight into the application of QED on neutron star evolution and modeling.

REFERENCES

- [1] Abbott, R., T. D. Abbott, S. Abraham, F. Acernese, K. Ackley, C. Adams, R. X. Adhikari, et al. “GW190814: Gravitational Waves from the Coalescence of a 23 Solar Mass Black Hole with a 2.6 Solar Mass Compact Object.” *The Astrophysical Journal* 896, no. 2 (June 23, 2020): L44. <https://doi.org/10.3847/2041-8213/ab960f>.
- [2] Anglani, R., M. Mannarelli, G. Nardulli, and M. Ruggieri. “Neutrino Emission from Compact Stars and Inhomogeneous Color Superconductivity.” *Physical Review D* 74, no. 7 (October 11, 2006): 074005. <https://doi.org/10.1103/PhysRevD.74.074005>.
- [3] Annala, Eemeli, Tyler Gorda, Alekski Kurkela, Joonas Näätä, and Alekski Vuorinen. “Quark-Matter Cores in Neutron Stars.” *ArXiv:1903.09121 [Astro-Ph, Physics:Hep-Ph, Physics:Nucl-Th]*, March 21, 2019. <http://arxiv.org/abs/1903.09121>.
- [4] Annala, Eemeli, Tyler Gorda, Alekski Kurkela, and Alekski Vuorinen. “Gravitational-Wave Constraints on the Neutron-Star-Matter Equation of State.” *Physical Review Letters* 120, no. 17 (April 25, 2018): 172703. <https://doi.org/10.1103/PhysRevLett.120.172703>.
- [5] Ashworth, W.B. “A Probable Flamsteed Observation of the Cassiopeia A Supernova.” *Journal for the History of Astronomy, Vol. 11, P. 1, 1980*, 1980. <https://doi.org/10.1177/002182868001100102>.
- [6] Bedaque, Paulo F., Sanjay Reddy, Srimoyee Sen, and Neill C. Warrington. “Neutrino-Nucleon Scattering in the Neutrino-Sphere.” *Physical Review C* 98, no. 1 (July 31, 2018): 015802. <https://doi.org/10.1103/PhysRevC.98.015802>.

- [7] Brooks, Craig Lee. “QUANTUM MAGNETIC COLLAPSE IN NEUTRON STAR BINARY SYSTEMS,” n.d., 84.
- [8] Burrows, Adam S. “Baade and Zwicky: ‘Super-Novae,’ Neutron Stars, and Cosmic Rays.” *Proceedings of the National Academy of Sciences* 112, no. 5 (February 3, 2015): 1241. <https://doi.org/10.1073/pnas.1422666112>.
- [9] Carroll, Bradley, and Dale Ostlie. *An Introduction to Modern Astrophysics*. Pearson, 2006.
- [10] Collins, Harry. *Gravity’s Kiss: The Detection of Gravitational Waves*. Cambridge, MA: The MIT Press, 2018.
- [11] Damour, Thibault. “1974: The Discovery of the First Binary Pulsar.” *Classical and Quantum Gravity* 32, no. 12 (June 25, 2015): 124009. <https://doi.org/10.1088/0264-9381/32/12/124009>.
- [12] Giacconi, Riccardo. “THE DAWN OF X-RAY ASTRONOMY,” n.d., 23.
- [13] Gold, T. “Rotating Neutron Stars as the Origin of the Pulsating Radio Sources.” *Nature* 218 (1968): 731–32. <https://doi.org/10.1038/218731a0>.
- [14] Haberl, F. “The Magnificent Seven: Nearby Isolated Neutron Stars with Strong Magnetic Fields.” *ArXiv:Astro-Ph/0510480*, October 17, 2005. <http://arxiv.org/abs/astro-ph/0510480>.
- [15] Hewish, A, J Bell, and J Pilkington. “Observation of a Rapidly Pulsating Radio Source.” *Nature* 217 (1968): 709–13. <https://doi.org/10.1038/217709a0>.
- [16] Klus, Helen, Elizabeth S. Bartlett, Antony J. Bird, Malcolm Coe, Robin Corbet, and Andrzej Udalski. “Swift J045106.8-694803; a Highly Magnetised Neutron Star in

the Large Magellanic Cloud.” *ArXiv:1210.7680 [Astro-Ph]*, December 6, 2012.

<http://arxiv.org/abs/1210.7680>.

- [17] Lattimer, J. M., and M. Prakash. “The Physics of Neutron Stars.” *Science* 304, no. 5670 (April 23, 2004): 536–42. <https://doi.org/10.1126/science.1090720>.
- [18] Lattimer, James M. “Introduction to Neutron Stars,” 61–78. Sinaia, Romania, 2015. <https://doi.org/10.1063/1.4909560>.
- [19] Margalit, Ben, and Brian D. Metzger. “Constraining the Maximum Mass of Neutron Stars from Multi-Messenger Observations of GW170817.” *The Astrophysical Journal* 850, no. 2 (November 21, 2017): L19. <https://doi.org/10.3847/2041-8213/aa991c>.
- [20] Masood, S.: Renormalization of QED near decoupling temperature. *Phys. Res. Int.* 2014, 48913 (2014). arXiv:1407.1414
- Ahmed, K.; Masood, S.S.: Finite-temperature and-density renormalization effects in QED. *Phys. Rev. D* 35, 4020 (1987). <https://journals.aps.org/prd/abstract/10.1103/PhysRevD.35.4020>
- [21] Masood, Samina S. “Electromagnetic Waves in Hot and Dense Media,” n.d., 19.
- [22] Masood, Samina S. “Neutrino Physics in Hot and Dense Media.” *Physical Review D* 48, no. 7 (October 1, 1993): 3250–58. <https://doi.org/10.1103/PhysRevD.48.3250>.
- [23] Masood, Samina S. “Nucleosynthesis in Hot and Dense Media.” *Journal of Modern Physics* 05, no. 05 (2014): 296–308. <https://doi.org/10.4236/jmp.2014.55040>.
- [24] Motte, Frederique, Sylvain Bontemps, and Fabien Louvet. “High-Mass Star and Massive Cluster Formation in the Milky Way.” *Annual Review of Astronomy and*

Astrophysics 56, no. 1 (September 14, 2018): 41–82.

<https://doi.org/10.1146/annurev-astro-091916-055235>.

- [25] Nadyozhin, D.K. “Gamow and the Physics and Evolution of Stars.” *Space Science Review* 74 (1995): 455–61. <https://doi.org/10.1007/BF00751432>.
- [26] Nicholl, M, P.K. Blanchard, and E Berger. “An Extremely Energetic Supernova from a Very Massive Star in a Dense Medium.” *Nature Astronomy*, 2020.
<https://doi.org/10.1038/s41550-020-1066-7>.
- [27] Oppenheimer, J. R., and G. M. Volkoff. “On Massive Neutron Cores.” *Physical Review* 55, no. 4 (February 15, 1939): 374–81.
<https://doi.org/10.1103/PhysRev.55.374>.
- [28] Ozel, Feryal, and Paulo Freire. “Masses, Radii, and Equation of State of Neutron Stars.” *Annual Review of Astronomy and Astrophysics* 54, no. 1 (September 19, 2016): 401–40. <https://doi.org/10.1146/annurev-astro-081915-023322>.
- [29] Pacini, F. “Rotating Neutron Stars, Pulsars and Supernova Remnants.” *Nature* 219 (1968): 145–46. <https://doi.org/10.1038/219145a0>.
- [30] Page, Dany, and A. Sarmiento. “Surface Temperature of a Magnetized Neutron Star and Interpretation of the *ROSAT* Data. II.” *The Astrophysical Journal* 473, no. 2 (December 20, 1996): 1067–78. <https://doi.org/10.1086/178216>.
- [31] Pathria, R.K., and Paul D. Beale. *Statistical Mechanics*. Elsevier, 2011.
- [32] Pavlov, G. G., V. E. Zavlin, B. Aschenbach, J. Trümper, and D. Sanwal. “The Compact Central Object in Cassiopeia A: A Neutron Star with Hot Polar Caps or a

Black Hole?” *The Astrophysical Journal* 531, no. 1 (March 1, 2000): L53–56.

<https://doi.org/10.1086/312521>.

- [33] Popov, S. B., and M. E. Prokhorov. “Magnetars Origin and Progenitors with Enhanced Rotation.” *Monthly Notices of the Royal Astronomical Society* 367, no. 2 (April 1, 2006): 732–36. <https://doi.org/10.1111/j.1365-2966.2005.09983.x>.
- [34] Prakash, Madappa, Ignazio Bombaci, Manju Prakash, Paul J. Ellis, James M. Lattimer, and Roland Knorren. “Composition and Structure of Protoneutron Stars.” *Physics Reports* 280, no. 1 (February 1997): 1–77. [https://doi.org/10.1016/S0370-1573\(96\)00023-3](https://doi.org/10.1016/S0370-1573(96)00023-3).
- [35] Rowan, Sheila, and Jim Hough. “Gravitational Wave Detection by Interferometry (Ground and Space).” *Living Reviews in Relativity*, n.d., 41.
- [36] Schmidt, M. “3C 273 : A Star-Like Object with Large Red-Shift.” *Nature* 197 (1963): 1040. <https://doi.org/10.1038/1971040a0>.
- [37] Schreier, E. “Evidence for the Binary Nature of Centaurus X-3 from UHURU X-Ray Observations.” *Astrophysical Journal* 172 (1972). <https://doi.org/doi:10.1086/180896>.
- [38] Sciamia, D, and M Rees. “Absorption Spectrum of 3C 9.” *Nature* 212 (1966): 1001–2. <https://doi.org/10.1038/2121001a0>.
- [39] Sedrakian, Armen, and John W. Clark. “Superfluidity in Nuclear Systems and Neutron Stars.” *ArXiv:1802.00017 [Astro-Ph, Physics:Cond-Mat, Physics:Nucl-Th]*, January 31, 2018. <http://arxiv.org/abs/1802.00017>.

- [40] Shapiro, Stuart, and Saul Teukolsky. *Black Holes, White Dwarfs, and Neutron Stars: The Physics of Compact Objects*. Wiley-VCH, 1983.
- [41] Steiner, Andrew W., James M. Lattimer, and Edward F. Brown. “The Neutron Star Mass-Radius Relation and the Equation of State of Dense Matter.” *The Astrophysical Journal* 765, no. 1 (February 12, 2013): L5.
<https://doi.org/10.1088/2041-8205/765/1/L5>.
- [42] Tauris, Thomas M. “Recycled Pulsars: Spins, Masses and Ages.” *ArXiv:1606.05117 [Astro-Ph]*, June 16, 2016. <http://arxiv.org/abs/1606.05117>.
- [43] Wang, Chencan, Jinniu Hu, Ying Zhang, and Hong Shen. “Properties of Neutron Star Described by a Relativistic β -Initio Model.” *ArXiv:2006.02007 [Astro-Ph, Physics:Nucl-Th]*, June 2, 2020. <http://arxiv.org/abs/2006.02007>.
- [44] Williams, D.E.G., and K Goto. “The Chemical Potential of an Electron Gas.” *Journal of Physics A: General Physics* 3 (1970). <https://doi.org/10.1088/0305-4470/3/5/014>.
- [45] Woltjer, L. “X-Rays and Type I Supernovae.” *Astrophysical Journal* 140 (1964).
<https://doi.org/doi:10.1086/148028>.
- [46] Yakovlev, Dmitry G., Pawel Haensel, Gordon Baym, and Christopher J. Pethick. “Lev Landau and the Conception of Neutron Stars.” *Physics-Uspekhi* 56, no. 3 (March 31, 2013): 289–95. <https://doi.org/10.3367/UFNe.0183.201303f.0307>.